LABORATORI NAZIONALI DI FRASCATI
SIS – Pubblicazioni

LNF– 94/055 (P)
26 Settembre 1994

DAΦNE Machine Project

Contributions to the
Fourth European Particle Accelerator Conference (EPAC 94)
Queen Elizabeth II Convention Centre, London, 27 June – 1st July, 1994

CONTENTS

Review of Φ-Factories

Mario Serio, Gaetano Vignola, DAΦNE Project Team [1]
INFN, Laboratori Nazionali di Frascati (LNF) - 00044 Frascati (Roma) - Italy

Abstract

The main accelerator physics and technology issues of electron-positron Φ-Factories are discussed. Advantages and drawbacks of possible colliding schemes are reviewed. The most relevant technological issues at DAΦNE, now under construction at LNF, are discussed.

1. INTRODUCTION

1.1 Energy frontiers vs. Luminosity frontiers.

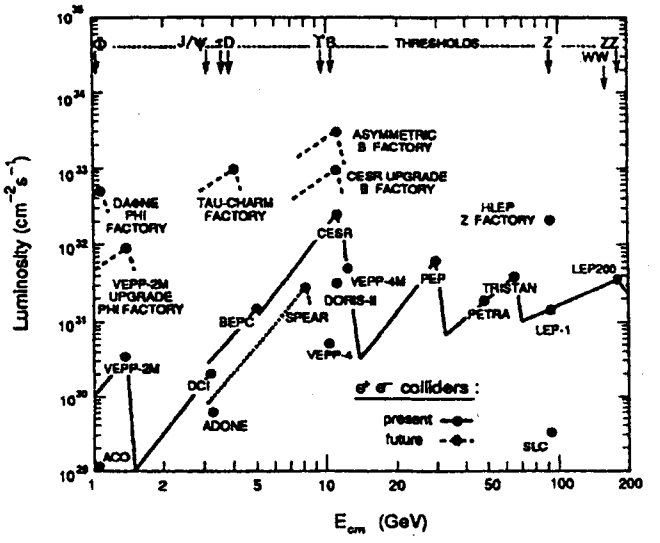

Figure 1 - Luminosity of present and future e^+e^- colliders and factories in the range 1÷200 GeV (from Ref. [2]).

In the last years, besides the continuing interest of physicists towards physics at colliders with higher and higher energy, considerable interest has developed towards very high precision measurements and in particular to the study of CP violation on colliders optimized and running at specific $s\bar{s}$ or $b\bar{b}$ resonances such as Φ, Υ, etc. The prerequisite to the realization of these colliders is abundant production of Φ or Υ particles reliably around the clock, hence the name *factories*.

In contrast to colliders at the energy frontiers, where huge financial effort, large international collaborations and large laboratories set the typical scale, in the race to very high luminosity at relatively low energy, the typical scale can well be that of a medium size national/regional Laboratory (e.g., LNF) and the financial effort is in most cases affordable by a single Institution.

The composition and the numeric consistency of both the physics and accelerator groups is not such to pose serious sociological and logistic problems, as often is the case with large collaborations.

The exploitation of local facilities, skills and experiences certainly affect the approach, making the design somehow site-dependent; new ideas and considerable R&D are nevertheless solicited.

1.2 Physics at a Φ-Factory

The realization of factories at the Φ energy (~1 GeV c.m.) has been proposed at several laboratories. The main motivation for a Φ-Factory is that it can provide a method to measure the ratio of the CP violating parameters ε'/ε with a precision of ~ $5\ 10^{-4}$ [3]. To fulfill the experimental requirements in order to verify CP violation, the yield of Φ particles necessary must be of the order of $\sim 10^{10}$/year. Then, given the peak cross section at the Φ resonance, $\sigma_{peak} = 4.4\times10^{-30}$ cm^2 and assuming 10^7 sec of operating time in one year, the average luminosity $<\mathcal{L}>$ must be $\sim 2.3\times10^{32}$ cm^{-2} sec^{-1}. To date, the maximum luminosity attained at the Φ energy is that of VEPP-2M, 4.3×10^{30} [4]. A luminosity improvement of about two orders of magnitude is then necessary.

2. LUMINOSITY STRATEGIES

Being the luminosity $\mathcal{L}$ the primary and most distinctive feature of a Φ-Factory, a brief digression is in order.

The luminosity per interaction point (IP) is, by definition:

$$\mathcal{L} = f\frac{N^+N^-}{\Sigma} = f\frac{N^+N^-}{4\pi\sigma_x\sigma_y}\ [\text{cm}^{-2}\,\text{sec}^{-1}]\,, \qquad (1)$$

with f the crossing frequency, N_{+-} the number of particles in the positron and electron beam, Σ the superposition area and $\sigma_{x,y}$ the rms horizontal and vertical beam sizes at the IP, assuming gaussian shape and head-on collision.

We make some simplifying assumptions: beams are bunched and h different bunches per beam collide at the IP; the number of particles per bunch N and the horizontal and vertical beam sizes are equal in both beams. The collision frequency is $f = h\, f_{rev}$, with f_{rev} the revolution frequency.

The single bunch luminosity $\mathcal{L}_o$ is limited by the beam-beam interaction. When two bunched beams collide, one bunch feels a focusing effect from the other, whose strength is described by the so called beam-beam tune shift parameter ξ:

$$\xi_{x,y} = \frac{r_e\, N\, \beta_{x,y}}{2\pi\,\gamma\,\sigma_{x,y}\,(\sigma_x + \sigma_y)}\,, \qquad (2)$$

with r_e the classical electron radius, $\beta_{x,y}$ the betatron functions at the IP, and γ the particle energy in units of rest mass. There is experimental evidence of a limit on the maximum value that ξ can take, beyond which the beam-beam effect is so strong that instability and beam blow-up occur and the lifetime and the luminosity are substantially reduced.

We can express the luminosity as:

$$\mathcal{L} = h\mathcal{L}_o = h\, f_{rev}\frac{N\,\gamma\,\xi_y}{2r_e\,\beta_y}\,(1+\frac{\sigma_y}{\sigma_x})\,. \qquad (3)$$

Equal tune shift in both planes ($\xi = \xi_x = \xi_y$) is obtained when:

$$\text{Emittance ratio} = \kappa = \kappa_\beta = \frac{\beta_y}{\beta_x} \rightarrow \frac{\sigma_y}{\sigma_x} = \kappa\,.$$

Under this condition the luminosity can be written as:

$$\mathcal{L} = h\mathcal{L}_0 = h\, f_{rev}\, N \left(\frac{\gamma}{2r_e}\right) \frac{\xi}{\beta_y} (1+\kappa). \qquad (4)$$

By inspection of the simple formula (4) we can identify the relevant parameters that could be pushed to limit to improve the luminosity. None is without limitation or drawbacks, however. Let's review them briefly.

2.1 Revolution frequency f_{rev}.

The size of the typical detector cannot be much smaller than 3+5 m, imposing a limit on the ring circumference to no less than ~20 m, corresponding to a revolution frequency of ~15 MHz. Assuming a filling factor <~0.5 for the bending magnets, one readily arrives at very intense bending fields, and small bending radii, with strong non-linear components which tend to reduce the dynamic aperture.

In addition, a substantial fraction of the machine length must be dedicated to RF, injection, beam instrumentation etc., which adversely affect the longitudinal coupling impedance with a larger relative weight than in a longer machine. In small rings, coherent synchrotron radiation is the source of non negligible *vacuum* impedance.

2.2 Number of bunches h.

Increasing the number of bunches has the nasty side-effect of parasitic crossings outside the interaction region (IR), which contribute to the beam-beam tune shift parameter, but not to the useful luminosity. Parasitic crossings can be eliminated by means of electrostatic separators, but in this case, the maximum number of bunches is limited by the constraint of having at least one half betatron wavelength between two parasitic crossing points. It is possible to go around this problem by adopting a scheme with two separate rings, tangent at the IP(s). The problem of avoiding parasitic crossing is circumvented in this way, except for the common part of the two storage rings, where in any case the beams must be kept separated either by electrostatic separators, or by accepting to collide at small angle. In case of separated rings, it is a reasonable choice to make the ring size larger, with many bunches, keeping the number of particles per bunch relatively small. Multibunch instabilities, however, can pose a serious limit because of the high total current.

2.3 β-function at the IP

A very small value of β at the IP has strong impact on the whole ring lattice design. First of all, in order to leave sufficient material-free solid angle to the detector, the first quadrupoles cannot be too close to the IP. The betatron function grows parabolically, taking a very large value at the quadrupole. The chromaticity is strongly affected and a powerful sextupolar correction must be provided elsewhere in the ring, with a corresponding reduction of dynamic aperture.

Also important, due to the parabolic increase of β around the IP, the transverse size increases along the bunch length and to keep the advantage of having small dimensions at the IP, the bunch length σ_l must be shorter or at most of the same order of β, otherwise geometric reduction of the luminosity occurs, the so called hour-glass effect. To achieve short bunch length puts an heavy burden on the RF system and on the machine impedance budget. Malignant instabilities can arise because of the very high peak current.

2.4 Coupling κ

In spite of the theoretical factor of two increase in luminosity that one can get with round beams κ~1, this solution is seldom used.

To exploit full coupling requires the two β functions at the IP to be of the same order, with strong focusing in both planes: the chromaticity is increased and the sextupolar correction is more complicated and makes the ring lattice less flexible. Moreover, there is an additional difficulty in the design of the interaction region, where space is at a premium. This is the reason why practically all existing colliders adopt the flat beam scheme, with strong focusing only on the vertical plane. An alternative way to achieve equal (small) values at the IP is by means of strong solenoidal focusing.

2.5 Tune shift parameter ξ

A substantial luminosity increase can also be obtained by increasing ξ. Unfortunately, it seems not possible to achieve arbitrarily large values of ξ without incurring in serious limitations. Besides the physical mechanism of the ξ limitation, which is very involved and far from having been solved theoretically in a conclusive way, there is an experimental experience over most existing and past colliders that the maximum ξ achievable is much like an universal constant. Namely, averaging over most electron colliders: $\xi \sim 0.04 \pm 0.015$.

According to theoretical arguments and simulations [5,6], there could be a net gain in the maximum ξ by adopting the round beam scheme, although there is not general consensus on this conclusion [7].

We cannot overestimate the relevance of experimental data on this very crucial issue. At the time of writing, the only one experiment made at CESR [8] has not dramatically confirmed the goodness of the round beam approach, even though, for various reasons, the experimental conditions were not very favorable and this datum has not to be considered conclusive in any way.

There is a very interesting plan of making round beams at VEPP2M [9] with a solenoidal focusing scheme similar to that proposed for the INP Φ-Factory [10]. In this way the possibility of increasing the beam-beam limit with round beams will be tested and hopefully validated in a realistic context.

Of course, all the above parameters are not free, affecting each other in several respects and confronting with other possible limitations of the storage ring design.

Not less important than the maximum luminosity is the luminosity lifetime. In addition to the peak luminosity, which is a qualifying figure, also the time between successive fills of the ring(s) is very important for a "practical" experiment to take data.

3. OVERVIEW OF Φ-FACTORIES

In this section we review the proposals and projects for Φ-Factories in the world. The main parameters relevant to the luminosity are summarized in Table I.

3.1 UCLA

The UCLA Φ-Factory design [11] consists of a compact race-track storage ring of 17 m circumference, equipped with 6 superconducting dipoles of 4T with large good field region and no curvature for simplicity of realization and reduction of cost.

Table I - Summary of luminosity related parameters of Φ-Factories

	INP	UCLA *	DAΦNE	KEK
Design Luminosity $\mathcal{L}$ (cm^{-2} sec^{-1}) ($\times 10^{32}$)	10	3. (10)	1.3 ->5.	30.
Design Luminosity/bunch $\mathcal{L}_o$ ($\times 10^{32}$)	10	3. (10.)	0.043	0.1
Total current lifetime (min)	11	45	230	15
Beam-Beam contribution to lifetime (min)	11	100	1500	600
Circumference (m)	35.2	17.4	97.7	120
Number of rings	1	1	2	2
Number of IRs	1	1	1 + (1)	1
Crossing type	Head-on	Head-on	H. angle	H. angle
Crossing half angle (mrad)	0	0	10÷15	20
Number of bunches per beam	1->3	1	30 ->120	300
Number of particles per bunch ($\times 10^{10}$)	20.	40. (16.)	9.	6
Momentum compaction factor α	.03 - .06	.11 (~0)	.005	.007
Horizontal β at IP (cm)	1.	19	450.	100.
Vertical β at IP (cm)	1.	3.9 (0.3)	4.5	1.
RMS Bunch length (mm)		30 (<3)	30	4.7
Energy loss (radiation) per turn (KeV)	32.1	14.1	9.3	14.5
Horizontal emittance (mm×mrad)	.47	3.2 (1)	1.	1.14
Coupling factor κ	1	0.2	0.01	0.01
Tune shift parameter ξ	>0.1	0.05	0.04	0.03

* Numbers in parenthesis refer to Phase 2 (QIR).

A sketch of the proposed layout is given in Fig. 2. One of the two straight sections is occupied by the RF cavity, the other one by a *small* detector. In the UCLA proposal an initial luminosity: $\mathcal{L} = 3\times10^{32}$ cm^{-2} sec^{-1} is achievable working with single bunches of 4×10^{11} particles, high emittance, $\kappa = 0.2$ and a rather conventional low-β interaction region. Due to the very compact design, special sextupoles are employed to correct the chromaticities.

At a second stage the lattice will be modified to obtain a "Quasi Isochronous Ring" (QIR) with a design luminosity $\mathcal{L} = 10^{33}$ cm^{-2} sec^{-1}. The idea is to shorten the bunch to the millimeter range by making the first order momentum compaction vanish, enabling very small values of the vertical betatron function at the IP, so that, even with a lower current (1.6×10^{11} particles), a higher luminosity can be obtained.

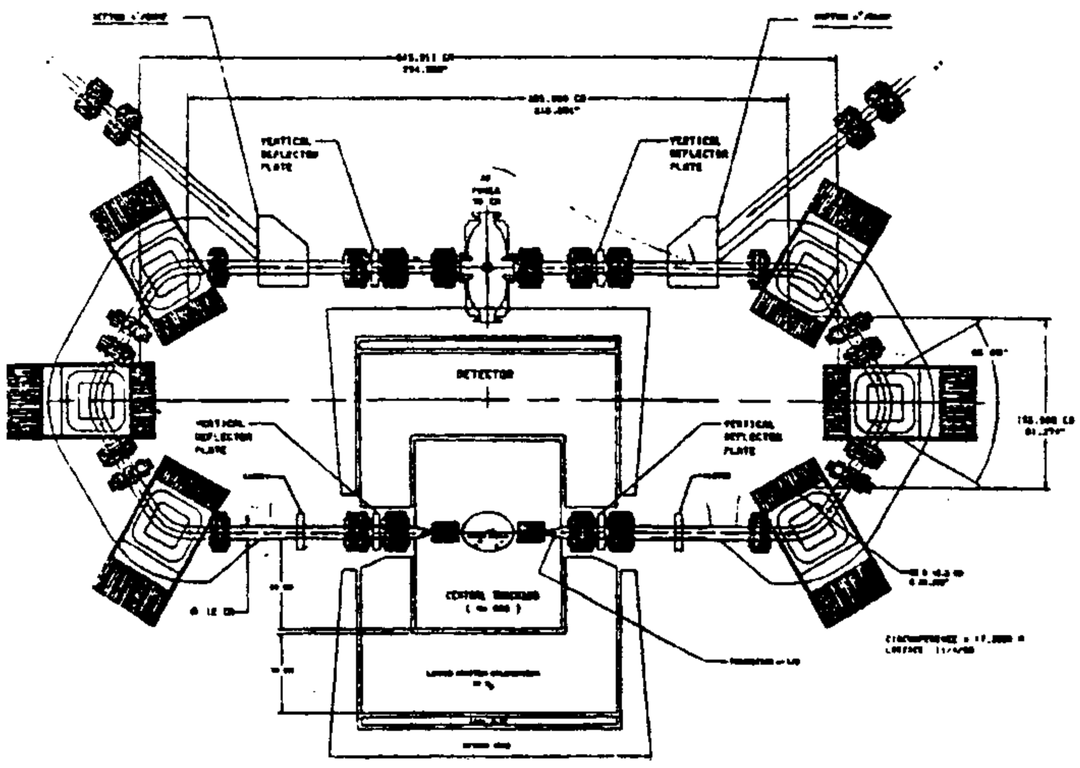

Figure 2 - Sketch of the UCLA Φ-Factory

3.2 INP

The Φ-Factory under construction at INP, Novosibirsk [10], undoubtedly incorporates the most innovative and exotic design ideas. It is 35 m long and has a rather peculiar "figure of eight" shape (see Fig. 3). One bunch per beam circulates in the machine and the collision points merge in the central part, allowing the bunches to cross at the same IP two times per revolution.

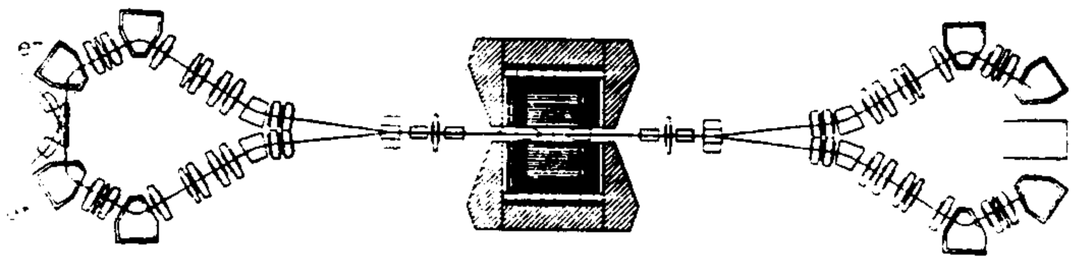

Figure 3 - Sketch of the INP Novosibirsk Φ-Factory

The number of particles/beam is 2×10^{11}, corresponding to an average current of ~ 270 mA/beam. An essential feature of the project is the strong solenoidal focusing: superconducting solenoidal magnets of 11 T, incorporated within the detector, are used to obtain equal low-β values of ~1 cm at the IP and, at the same time, to exchange the horizontal and vertical planes at each crossing, creating the same emittance in the two planes. The bending magnets are also superconductive at 6.5 T.

The first-stage luminosity design is 10^{33} cm^{-2} sec^{-1} in the single bunch mode. This ultra high luminosity can be reached exploiting the round beam option, with the operating point on the main coupling resonance with no degeneration of the normal modes of oscillation. The design is based on the idea that round beams can get a value of ξ_{max} higher than 0.1 in both planes.

A second stage is foreseen, with up to three bunches and electrostatic separation at unwanted IPs. The luminosity at this stage will improve by a factor 3÷10.

The lifetime is of the order of few minutes and therefore injection at 0.1÷0.2 Hz is planned.

The project is supported by the Russian Government within the State Program on High Energy Physics, but the financing plan has been drastically detained and INP has to support the project within its own budget.

3.3 DAΦNE and KEK

The INFN-LNF project DAΦNE [12] and the KEK [13] proposal are similar. They both exploit existing buildings and facilities and use the same approach of storing many bunches (≤120 and ≤ 300, respectively) in two separate rings ~100 m long. The beams are very flat and are brought to collision at a horizontal angle.

The approach is based on conventional techniques, normal conducting (NC) dipole magnets, high field NC wigglers and room temperature RF cavities.

In the KEK project the two rings are superposed, with two long straight sections (SS), one for the IR, the other for the RF, and two short sections, one for injection and the other for the feedbacks.

DAΦNE adopts a different solution in that the rings lay in the same plane and are asymmetric with a short and a long half. Two IRs can be accommodated. The crossing angle can be changed by powering a small dipole, located after the splitter magnet that separates the trajectories of the two beams.

The short SS is used for the RF and the feedback systems, the long one for injection.

In both projects the lattice is a modified Chasman-Green. The wigglers, accommodated in dispersive regions in the arcs, are used to increase the radiation and to control the emittance.

4. STATUS OF DAΦNE

DAΦNE has been approved and funded in 1990; the detailed engineering design started in 1991 and the construction is proceeding steadily. A general description of the facility has been given in [12]. The beginning of the commissioning is scheduled by 1996.

The initial effort is concentrated to ensure the accumulation of at least 30 + 30 bunches for an initial routine luminosity $\mathcal{L} = 1.3\ 10^{32}\ cm^{-2}\ sec^{-1}$.

In the following sections we give the status of the principal systems.

Detailed information on the various subsystems are found in other papers presented at this Conference.

4.1 Injector

A powerful, reliable and stable injection system has been recognized as a very important requisite to get the target average luminosity, because of the rather high number of positrons and electrons to store (up to 10^{13} in ~5 min) and of the necessity of frequent injections.

The injector complex consists of an e^+/e^- Linac, an Accumulator/damping ring and transfer lines. All the components of the injection chain can operate at full energy and top-up injection is foreseen, to keep the average luminosity high.

The Linac can deliver e^+/e^- beams at 50 Hz. It is now under test at Titan-Beta [14] and the installation at LNF will begin by the end of 1994.

The 32.56 meter long Accumulator/damping ring is used to accumulate at 50 pps the required number of electrons (positrons) in one RF bucket and to damp the transverse and longitudinal emittance of the Linac beam.

The damped beam is extracted at ~1 Hz and injected into a single bucket in the main ring. This solution avoids saturation of injection and the aperture requirements for injection in the main rings are relaxed.

Magnetic channels transfer the beams from the Linac to the Accumulator and from the Accumulator into the main rings, snaking inside the already existing tunnels and buildings around Adone, now dismantled (see Fig. 4).

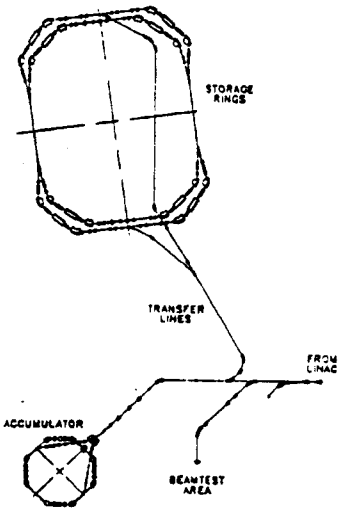

Figure 4 - Layout of DAΦNE and injector

The Accumulator and transfer lines are now under construction by Oxford Instuments and Ansaldo respectively, and the commissioning will start in 1995.

4.2 Emittance Wiggler

Four NC 1.8 T, 2 meters long, 40 mm gap, wiggler magnets are present in each ring, to increase the radiated energy. In addition, by slightly changing the optical functions in the wigglers, it is possible to tune the beam emittance over a wide range without deteriorating the damping time.

A wiggler prototype built by Danfysik (Denmark) has been delivered to LNF, and after a complete set of measurements, the authorization has been released for series production, with some modification suggested by the tests.

The magnetic quality of the wiggler meets the requirements of the DAΦNE Main Rings. Numerical simulations confirm that perturbation introduced by integrated sextupolar term in the wigglers is not harmful.

4.3 Vacuum System

The total pumping speed installed on each storage ring is a huge 125000 l/s over 100 meters of vacuum chamber. The main ring vacuum system is dimensioned for an operating pressure of 1 nTorr with ~ 5 Amp of circulating current. It is also required to have a rapid recovery of operating pressure after an intervention in the vacuum chamber or after an accident.

The vacuum system is based on Ti sublimation pumps (TSP) located in the vacuum antechamber of the arc sections, right close to copper absorbers. In addition, sputter ion pumps are used to pump down CH_4 and noble gasses.

Different surface finishing and treatments on two Al 5083 prototypes of the arc vacuum chamber have been investigated. Using the obtained results, which confirmed our choices, the cleaning procedures and the operational procedure for the flashing of Ti filaments in the TSPs have been assessed.

Detailed specifications for the arc vacuum chamber are completed and the contract for the fabrication awarded.

4.4 RF

The first main ring cavity is now under construction. Because of the large current and large number of bunches, the reduction of the beam-cavity spectra interaction is the most demanding feature of the DAΦNE RF system.

The RF cavity design aimed at significantly reduce the impedance of the high order cavity modes (HOM) by a proper shape of the resonator and, more effectively, by coupling off the HOM electromagnetic fields with waveguides.

The waveguide, whose cutoff frequency is higher than that of the accelerating mode, are connected to the cavity surface and terminated to 50 Ω on the other side, by means of broadband (0.5÷3 GHz) waveguide to coaxial transitions under vacuum, which have been developed at LNF [15] to this purpose. This solution avoids the use of RF lossy materials within the waveguides, in the ultra high vacuum of the accelerator.

This system has been tested on a cold prototype and the measured HOM Qs are below those required to damp multibunch instabilities with our bunch-by-bunch feedback system.

The RF power source at 368.25 MHz is a 150 kW/CW TH2145 klystron amplifier developed by Thomson Tube Electronique and successfully factory tested at full power. The estimated beam power is ~100 kW at the full design current.

4.5 Interaction Region

One of the two IRs will accommodate the detector KLOE [3], designed mainly to study CP in neutral K decays. The other one is assigned to a smaller detector FINUDA [16], designed to study hypernuclei formation and decay. The KLOE construction is in a more advanced status.

The KLOE interaction region is 10 m long. The low-β quadrupole triplets, of permanent type, are 46 cm far from the IP and are confined in a cone of 9° half aperture, leaving a material-free solid angle for the apparatus of ~ 99%. The first 2 quadrupoles of the triplets have already been built by Aster Enterprises and the measured field quality exceed our specifications. It is a requirement of the experiment to have a large (radius ~ 10 cm) aperture vacuum chamber at the IP as transparent as possible to the produced particles. The outer parts of the IR vacuum chamber are made of stainless steel with a copper coating inside to reduce the ohmic losses.

The inner section, bulb-shaped at the IP, is made of 0.5 mm thick pure beryllium, directly brazed onto the stainless steel pipe. Inside the spherical part of the chamber a 50 micron beryllium shield provides a continuous profile to the vacuum chamber to reduce RF losses. Water pipes, brazed as close as possible to the interaction point, provide the cooling needed to compensate for the thermal load on the vacuum chamber.

The supporting system consists of two independent structures: the detector support and the triplet assembly support, to allow relative freedom of mechanical alignment of the permanent magnet quadrupoles without affecting the detector. The detector supporting structure holds also the vacuum chamber.

The pumping system is a combination of lumped sputter ion pumps, distributed sputter ion pumps and non evaporable getter pumps. There are no pumps inside the detector near the IP.

The pumping system is able to reach a mean pressure of about $5 \cdot 10^{-10}$ Torr at full beam current after 2 or 3 months of conditioning.

5. REFERENCES

[1] The DAΦNE Project Team: S. Bartalucci, M. Bassetti, M.E. Biagini, G. Biscari, R. Boni, A. Cattoni, V. Chimenti, A. Clozza, S. De Simone, G. Di Pirro, A. Drago, A. Gallo, A. Ghigo, S. Guiducci, H. Hsieh, Q. Huamin, F. Marcellini, C. Marchetti, M.R. Masullo, M. Migliorati, C. Milardi, M. Modena, L. Palumbo, L. Pellegrino, M.A. Preger, G. Raffone, C. Sanelli, F. Sannibale, M. Serio, F. Sgamma, B. Spataro, A. Stecchi, L. Trasatti, C. Vaccarezza, M. Verola, M. Vescovi, S. Vescovi, G. Vignola, J. Wang, Y. Xianming, H. Yu, M. Zobov.

[2] J. Kirkby in "Frontiers of Particle Beams: Factories with e^+/e^- Rings" - Lecture Notes in Physics 425, Springer-Verlag, M. Dienes et al (Eds.), p. 381 (1992)

[3] The KLOE Collaboration, "KLOE, a general purpose detector for DAΦNE", Frascati Internal Note LNF-92/019 (IR), April 1992.

[4] P.M. Ivanov et al., "Luminosity and beam-beam effects on the electron positron storage ring VEPP-2M", in Proceedings of 3rd advanced ICFA beam dynamics workshop Novosibirsk 1989 - Ed. I. Koop and G. Tumaikin.

[5] S. Krishnagopal, R. H. Siemann, "Simulation of Round Beams", in Proceedings of 1989 IEEE Particle Accelerator Conference, Chicago 1989, p.836 (1989).

[6] N. S. Dikansky et al., "Incoherent Beam-Beam Effects for Round Beams in the Novosibisrsk Phi-Factory Project", in Proceedings of 1991 IEEE Particle Accelerator Conference, San Frascisco 1991, p.523 (1991).

[7] K. Hirata (CERN-KEK), "Round and Flat Beams in the Phi-factory", LNF Note Ares-15, 12/10/1989 (1989).

[8] P. Bagley et al, "Nearly Equal β* at CESR, Proceedings of 1991 IEEE Particle Accelerator Conference, San Frascisco 1991, p.467 (1991).

[9] A.N. Filippov et al., "Proposal of the Round Beam Lattice for VEPP-2M Collider", Proceedings of XVth International Conference on High Energy Accelerators, Hamburg1991, p. 1145 (1992).

[10] L. M. Barkov et al, "Status of the Novosibirsk Phi-Factory Project", in Proceedings of 1991 IEEE Particle Accelerator Conference, San Frascisco 1991, p.183 (1991).

[11] C. Pellegrini, The UCLA Φ-Factory Project, Proceedings of Workshop on Physics and Detectors for DAΦNE - Frascati, April 9-12 1991, p.83.

[12] DAΦNE Project Team, "DAΦNE Status Report", Proc. of 3rd EPAC Conference - Berlin, 1992.

[13] K. Hirata and K. Ohmi, "Feasibility of a Φ-Factory in KEK", 1991 Particle Accelerator Conference, San Francisco 1991, p. 2847 (1991).

[14] K. Whittam et al., "Design of the e+/e- Frascati Linear Accelerator for DAΦNE', in 1993 Particle Accelerator Conference, Washington D.C., USA, May 1993, pp. 611-613.

[15] R. Boni et al., "A Broadband Waveguide to Coaxial Transition for HOM Damping in Particle Accelerator RF Cavities", LNF 93/075(P), 1993 (to be published on Particle Accelerators).

[16] The FINUDA Collaboration, "FINUDA, a detector for nuclear physics at DAΦNE", Frascati Int. Note LNF-93/021 (IR), May 1993.

Overview of DAΦNE Beam Diagnostics

M. E. Biagini, C. Biscari, A. Drago, A. Ghigo, S. Guiducci, H. Hsieh, C. Marchetti,
M.R. Masullo*, C. Milardi, M.A. Preger, F. Sannibale, M. Serio, M. Vescovi, G. Vignola
INFN, Laboratori Nazionali di Frascati - 00044 Frascati (Roma) - Italy
*INFN, Sezione di Napoli, Mostra d'Oltremare, Pad. 20, 80125 Napoli - Italy

Abstract

A general overview of the diagnostics designed for each part of the DAΦNE complex is given. The relevant beam measurements we need to provide are: emittance, energy and energy spread in the Linac, longitudinal and transverse dimensions, beam position and tunes in the Accumulator and in the double ring collider, where overlap of the two beams at the interaction point has to be optimized and controlled.

1. INTRODUCTION

DAΦNE is a high luminosity electron-positron double ring collider [1], designed to serve as a Φ–factory (1020 MeV c.m.), now under construction at the INFN Frascati National Laboratory; its commissioning is foreseen in fall 1996.

The average luminosity must be improved by two orders of magnitude with respect to existing facilities in the same energy range to fulfill the requirements of the experiments, based on high precision measurements of CP violation related parameters. To achieve this goal, up to 120 bunches will be stored in each ring, collisions taking place in two low-β interaction points (IP), where the experimental detectors (KLOE [2] and FINUDA [3]) are installed. The ultimate total beam current is ≈2x5 A (≈10^{13} particles in each ring).

A full energy injection system, consisting of a 550 (e^+) / 800 (e^-) MeV Linac and an intermediate booster (Accumulator), provides topping-up capability. Injection from scratch of both beams will take place in 5+10 minutes, while half this time is expected in the topping-up mode. Transfer Lines drive the beam from the Linac to the Accumulator, and, after damping, from the Accumulator to the Main Rings.

The primary role of beam diagnostics is to make performance optimization easy. The stringent requirements of a high average luminosity collider call for careful control of life-time, beam sizes, coupling, storage rings optics, closed orbit distortion and stability of the interaction points. This can be accomplished only with extensive, redudant and general-purpose beam instrumentation.

Diagnostic devices will also be used for the initial commissioning of machine components and, in routine operation, to measure beam parameters at the boundaries between the injection chain elements, to check and optimize injection, extraction and transfer efficiency, and accumulation rate. This is very important in view of the fast filling rate required.

The table below summarizes the various types of beam instrumentation in the DAΦNE accelerator complex.

2. LINAC AND TRANSFER LINE INSTRUMENTATION

The DAΦNE Linac [4], is an electron/positron accelerator delivering 10 ns FWHM macropulses with nominal peak current of 40 mA (e^+) and 150 mA (e^-) at 50 pps. The diagnostic devices along the LINAC are sensitive to 1 mA.

The main parameters to be checked are emittance, central energy and energy spread of both beams.

Beam emittance is measured with the *three gradients method* [5]. The beam width is measured as a function of the gradient in a quadrupole of the Linac/Transfer Line matching section, by letting the beam strike a chrome-doped alumina flag downstream the quad. The emitted light, proportional to beam density, is collected by a CCD camera + frame grabber system and processed by the Main Control System to derive the horizontal and vertical emittances and optical functions at the quadrupole.

Energy measurements are performed by a spectrometer system [6], consisting of a small angle pulsed dipole magnet and a 60° DC dipole, with a secondary emission monitor (SEM) in its focus, made of 34 tungsten bars (90×2.7×2.7 mm^3 each) grouped to form a 24 channels hodoscope. Resolution is $\delta(\Delta E/E) = \pm 0.07\%$ (e-), $\pm 0.18\%$ (e+).

DAΦNE Beam Instrumentation Summary Table

		Storage Rings		Interaction Points		
Type	Tr.Lines	Acc.	e+/e-	DAY-1	KLOE	FINUDA
Secondary Emission (SEM) Hodoscope	1					
Faraday Cup	1					
Fluorescent Flag	18	2	2/2			
Slit/Scraper	4		3/3			
Beam Stopper	3					
Toroidal Current Monitor	9	1				
Wall Current Monitor		1				
DC current Monitor			1/1			
Beam Position Monitor - Stripline	23	4+1		12	4	4
Transverse Kicker - Stripline		1	2/2			
Beam Position Monitor - Button		8	36/36	13	6	6
Synchrotron Radiation Monitor		2	1/1			
H/V Tune Monitor/Tr. Feedback		2	2/2			
Synchrotron Tune Monitor/Long. Feedback		1	1/1			
Luminosity Monitor				2	1	1

The low repetition rate and intensity of the beam in the Transfer Lines require high sensitivity of the beam position monitors (BPM). Stripline monitors are used in the Transfer Lines and in the Accumulator to perform the measurement of the relatively weak and long current pulses entering the Accumulator from the Linac and the low repetition rate (~1 pps), high peak-current pulses from the Accumulator into the Main Rings.

The BPMs consist of four 50Ω strip electrodes, placed on opposite sides of the vacuum chamber horizontally and vertically (at 45° in the Accumulator), short circuited at one end inside the vacuum chamber. The strip length is ~0.15 m, with a response broadly resonating at 500 MHz. The output voltage is a doublet of pulses of opposite polarity, reproducing the longitudinal beam density, spaced by 1 nsec. Each electrode is separately connected through a good quality, high-frequency cable to the measuring electronics, thus allowing true single-pass acquisition of the beam position.

The detector is self-triggered and can be armed by the Master Trigger Generator to gate any selected single bunch passage, or used in free-run mode for stored beam measurements in the Accumulator.

The position detection is based on the amplitude to phase modulation-demodulation technique, where the amplitude ratio of two opposing electrodes, carrying the position information, is converted by means of a quadrature hybrid junction into a phase difference between two equal-amplitude signals. The BPM pulses are fed to a broad-band (~20 MHz bandwidth) band-pass filter ringing at 368 MHz (5-th harmonic of the Accumulator RF frequency). The pseudo-sinusoidal signals are then amplified and clipped by fast comparators. The phase difference is measured by an exclusive-OR circuit, whose average (low-pass filtered) DC output is proportional to the beam position.

The main advantages of such a detector are that it is self-normalizing, thus allowing a wide intensity range, and that it can be used both in single-pass and stored beam modes.

The intensity of the bunches injected into and extracted from the Accumulator is monitored by high performance toroidal current monitors [7].

Flags of fluorescent material (Beryllium Oxide) can be inserted in the vacuum pipe to intercept the beam at an angle of 45°. These screens are used to monitor the beam size and position, during the Transfer Lines set up, but they are not compatible with injection at full rate. A couple of them is provided in the injection/extraction septa of the Accumulator and the Main Rings.

In the Transfer Lines, slits can be inserted towards the center of the pipe, to reduce the aperture. They are used at suitable points to cut any portion of the beam outside the acceptance limit in order to prevent distributed beam spills.

3. ACCUMULATOR AND MAIN RINGS

3.1 Beam position

The beam position monitors are the primary diagnostic system in the Accumulator and Main Rings. The BPM system is based on the stripline monitors mentioned above and on electrostatic button monitors. Special BPMs, buttons and directional striplines are envisaged in the Interaction Regions to monitor the separation and crossing of the beams. Other stripline electrodes are used as longitudinal monitors and in the transverse feedback and tune monitor systems.

The highest precision and reproducibility are required in the Main Rings, where the monitors consist of four button electrodes mounted flush with the vacuum pipe. This design helps in maintaining coupling impedance and parasitic losses within acceptably low values in spite of the large number of units required. Three different designs, with different sensitivities and scale factors are present because of the varying cross-section of the vacuum chamber.

The BPM detector electronics is under development at LNF. It is a VXI board including an RF detector module and a digital section with two 12-bit ADCs and a DSP processor to compute the beam position. The last 2000 measurements are stored in a RAM memory on-board.

Two modes of operation are foreseen: single pass and stored beam. In both each button electrode is sequentially connected to the same RF detector by means of a PIN diode multiplexer. Therefore, four subsequent beam pulses are necessary to measure a single-pass position. A fast GaAs switch provides the capability to gate a particular bunch.

The voltage induced in each electrode is measured by heterodyning and detecting at an IF of 10.7 MHz the response of a tuned filter resonating at the RF frequency with a bandwidth of ~10 MHz. The IF signal goes to two separate circuits and is detected with synchronous demodulators. One part of the signal is low-pass filtered (f_C ~20KHz) prior to digitization for stored beam measurements; in the single pass mode, the detected IF signal is sampled and held in synchronism with the desired bunch passage, then digitized.

The beam position is computed from the cross-differences of the induced voltages normalized to the sum, to remove the current intensity dependence. The measurement rate is 1000/sec with the possibility of averaging over several subsequent passages of the stored beam, to improve resolution. Our goal is <2 mm*mA rms in the single passage and <0.01 mm in the stored beam mode (with 46 mA/bunch).

3.2 Beam current

In the Accumulator the total beam charge is monitored by an integrating toroidal current transformer [5]. It consists of a ceramic gap in the vacuum pipe, surrounded by a torus of high-frequency, high-μ ferrite. A conductive screen shielding the monitor prevents radiated noise. The monitor response is a ≈70 ns long pulse, largely independent of the transverse beam size and position and of the bunch duration, which can vary from ~10 nsec (Linac beam) to ~0.1 nsec (stored beam).

The pulse peak amplitude is proportional to the bunch charge and is measured by means of a sampler module [SRS, model SR255]. The charge measurement in the Accumulator is used to stop injection when a preset limit is reached, in order to evenly fill the Main Rings.

A DCCT is used in the Main Rings to yield a precise absolute measurement of the total circulating current.

3.3 Tune monitor

In the storage rings the fractional part of the betatron tunes ΔQ_x, ΔQ_y is measured by transversely exciting the beam at RF frequency with a pair of stripline kickers and measuring the (coherent) resonant beam response of the beam in the plane of excitation with a transverse pick-up and the (coherent and incoherent) beam enlargement with the SR monitor.

The sweeping excitation is provided by the RF output of a network analyzer, boosted to ≤100 W with a power amplifier; the coherent beam response is detected with the network analyzer or with the synchrotron radiation monitor.

The betatron tune monitor is part of the transverse feedback system, whereby the detected signal of a coherent beam oscillation is amplified and fed back with the appropriate phase to the beam by stripline kickers, to damp any transverse instability of the beam. The synchrotron tune is measured by phase-modulating the RF cavity and observing the longitudinal beam response with a longitudinal monitor.

Residual oscillations can also be observed with the same instrumentation. Both longitudinal and transverse Beam Transfer Functions (BTF) are measurable with these monitors.

3.4 Synchrotron Radiation Monitors

Both the Accumulator and the Main Rings are equipped with two synchrotron radiation monitors, one for each beam, used to measure the transverse and longitudinal beam size (the rms bunch length at full current is 30 mm).

In each one of the Main Rings the source point is in one of the parallel face dipole magnets [1], where the dispersion vanishes and the beam horizontal and vertical rms sizes are 2.5 mm and 0.28 mm respectively.

Measurements are performed within the visible range (400-600 nm) because it is possible to use high quality commercial optical components and detectors, maintaining a diffraction limit which sets the vertical resolution to 0.08 mm (4% error in the vertical beam width measurement).

The light from the beams is driven through two channels onto a common optical bench placed outside the Main Rings hall, to reduce to a minimum the number of remotely controlled adjustments. The transverse profiles are measured by means of a CCD camera and an image analyzer [8], GPIB connected to the Main Control System. The beam emittance is calculated from the measured widths and knowledge of the optical functions. The length of any individual bunch is measured with a 25 Ghz photodetector [9], directly connected to a sampling oscilloscope, and averaged over ~8000 turns.

The betatron tune distribution is also measured by exciting the beam and detecting the light through a slit with a photodiode [10]. This method is used to measure the incoherent contributions due to nonlinear forces in the rings such as ion trapping and beam-beam interaction.

3.5 Interaction point

An *absolute* luminosity measurement will be performed at both IPs by measuring the rate of single beam-beam bremsstrahlung [11]. A special vacuum chamber in the splitters [1] leaves enough free space for the γ rays to reach a thin window at the end of the magnets, within a cone of 3 mrad full aperture. Downstream the window a proportional counter, made of thin lead layers interleaved with scintillating fibers collects the photons and provides energy discrimination. Luminosity is calculated by dividing the measured counting rate by the theoretical integrated cross section. The photon flux, at the full DAΦNE design luminosity, is several MHz, so that the luminosity can be monitored continuously with high statistical precision. However, this measurement is not likely to be used as a feedback signal for the two beams overlap, since the luminosity is flat around its optimum.

A good probe for beam overlap optimization is instead the beam-beam deflection [12]: when the two beams cross at the IP with a vertical displacement between the two centers of mass, they are deflected towards each other. Figure 1 shows the deflection angle at the IP as a function of the distance between the two beams for the nominal DAΦNE parameters.

The beam-beam induced deflection propagates in the whole rings and can be measured at any BPM. In practice, it is convenient to leave a gap in one of the two beams in such a way that one can measure the difference in position between interacting and non interacting bunches. For the maximum foreseen deflection this difference ranges between ± 150 μm. By taking all BPMs in the ring one can improve the sensitivity of the measurement. At the design sensitivity it is possible to detect an overlap corresponding to a tune shift ten times smaller than the nominal one. This method can be exploited in a luminosity feedback system, since the beam deflection changes sign at the optimum overlap with a slope proportional to the linear beam-beam tune shift.

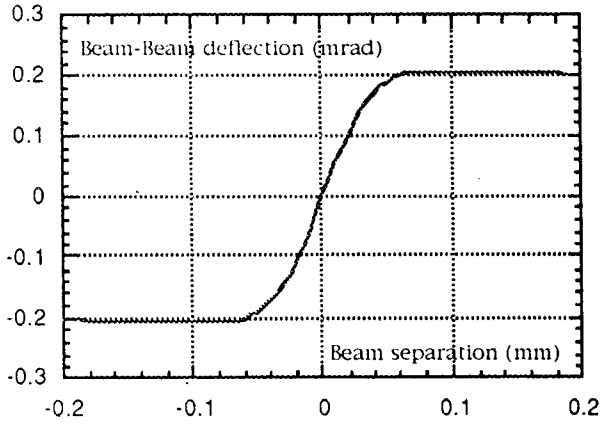

Figure 1. Beam-beam deflection angle.

4. REFERENCES

[1] G. Vignola, "DAΦNE, the Frascati Φ-Factory", in 1993 Particle Accelerator Conference, Washington, USA, May 1993, pp. 1993-1997.

[2] "KLOE, a general purpose detector for DAΦNE", Frascati Internal Note LNF-92/019 (IR), April 1992.

[3] "FINUDA, a detector for nuclear physics at DAΦNE", Frascati Internal Note LNF-93/021 (IR), May 1993.

[4] K. Whittam et al., "Design of the e+/e- Frascati Linear Accelerator for DAΦNE', in 1993 Particle Accelerator Conference, Washington D.C., USA, May 1993, pp. 611-613.

[5] F. Sannibale, "DAΦNE-LINAC beams emittance measurement design", DAΦNE Note LC-5, September 3, 1992.

[6] F. Sannibale and M. Vescovi, "LINAC to Accumulator area transfer line & DAΦNE-LINAC spectrometer", DAΦNE Note LC-3, February 1992.

[7] ICT-178-070-10:1 by BERGOZ-France.

[8] LBA 100 A by SPIRICON, Inc.- USA.

[9] 143X by New Focus, Inc - USA.

[10] M. E. Biagini et al.: "Observation of Ion Trapping at Adone", in XI-th International Conference on High Energy Accelerators, CERN - Geneva, July 1980, pp. 687-692.

[11] M. Preger, "A luminosity monitor for DAΦNE", DAΦNE Note IR-3, December 1993.

[12] M. Preger and M. Serio, "Luminosity optimization with beam-beam deflection", DAΦNE Note IR-4, January 1994.

Status of the DAΦNE RF System

R. Boni, A. Gallo, P. Baldini, F. Lucibello, S. Quaglia
INFN Laboratori Nazionali di Frascati,
C.P. 13, 00044 Frascati, Rome (Italy)

Abstract

The DAΦNE RF System consists of one quarter wave resonator in the pre-accumulator ring fed by a 73.65 MHz - 30 kW channel and one cavity per each main ring powered by a 368.25 MHz - 150 kW klystron. The main ring cavities are equipped with waveguides terminated by means of broadband adapters to 50 Ω loads to damp the High Order cavity Modes. This paper gives an overview of the status of the RF system and also briefly describes the low level RF control electronics.

1. INTRODUCTION

The Frascati Φ-Factory project DAΦNE [1] is now in a very advanced stage. The machine consists of two intersecting storage rings, for electrons and positrons respectively, to provide 1020 MeV e^+/e^- center of mass collisions at a maximum current of 5 Amps per beam with 120 bunches per ring. Full energy injection in both rings is performed with a 50 Hz linear accelerator [2] and a pre-accumulator damping ring. The positrons or electrons injected in the pre-accumulator are stored in a single bunch and extracted at 1 Hz and injected in the main rings.

Parameters and architecture of most components of the DAΦNE RF system are well defined. The prototypes of the RF cavities have been low power tested and ordered to the industry. The RF power supplies have been commissioned to industry as well.

2. THE ACCUMULATOR RING RF SYSTEM

The main parameters of the accumulator RF system are reported in Table I.

Table I
The Accumulator RF System Parameters

RF Frequency	73.65 MHz
Harmonic Number	8
Cavity Impedance ($V^2/2P$)	1.50 MΩ
Cavity Unloaded Q	22000
RF Peak Voltage	200 kV
Cavity Power	13.3 kW
Beam Current	130 mA
Beam Power	1.2 kW
Tetrode Power	30 kW

The cavity, made of oxygen free, high conductivity (OFHC) copper, is a 73.65 MHz quarter wave resonator [3] and is being manufactured by industry (CERCA, Romans, France). The shape of the cavity has been carefully studied to reduce the probability of vacuum resonant discharges (e.g. multipactoring) at high field levels. Tuning is accomplished by a plunger placed in the magnetic field region of the resonator; RF power is coupled with a magnetic loop. A drawing of the cavity is shown in Figure 1.

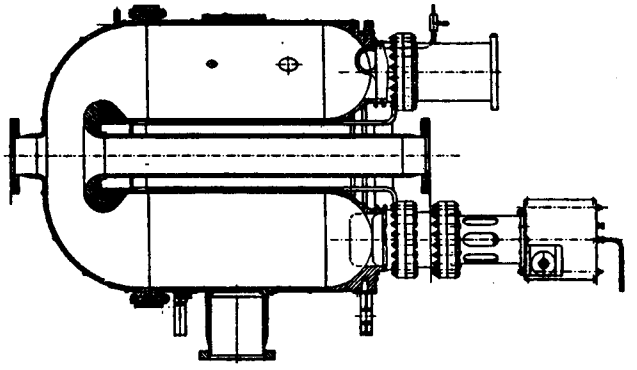

Figure 1. The Accumulator Ring RF Cavity

The RF power supply, to be placed 30 meters from the accumulator hall, is a 30 kW continuous wave (CW) water cooled tetrode tube driven by a 2 kW solid state amplifier (R&S, Berlin, Germany). It is connected to the cavity with a 6-1/8" coaxial line through a three port ferrite circulator which allows to safely operate the power final stage and reduces the risk of oscillations when the cavity is detuned to lower frequencies to meet the Robinson stability criterion.

The amplitude and phase of the RF cavity voltage together with the cavity tuning are controlled by dedicated servo loops. The frequency response of the amplitude and phase control loops has been improved by selecting fast and linear devices and a typical result is shown in Figure 2.

A gain higher than 60 dB at 50 Hz can be reached; any spurious modulation at that frequency can be reduced by a factor larger than 1000. Full computer interfacing of the RF chain is being developed. A current-feedback voltage-gain-controlled operational amplifier (Comlinear CLC 520) allows to remotely control the loop gains to improve the RF control system flexibility. Full control circuit tests have been performed on a low power cavity prototype.

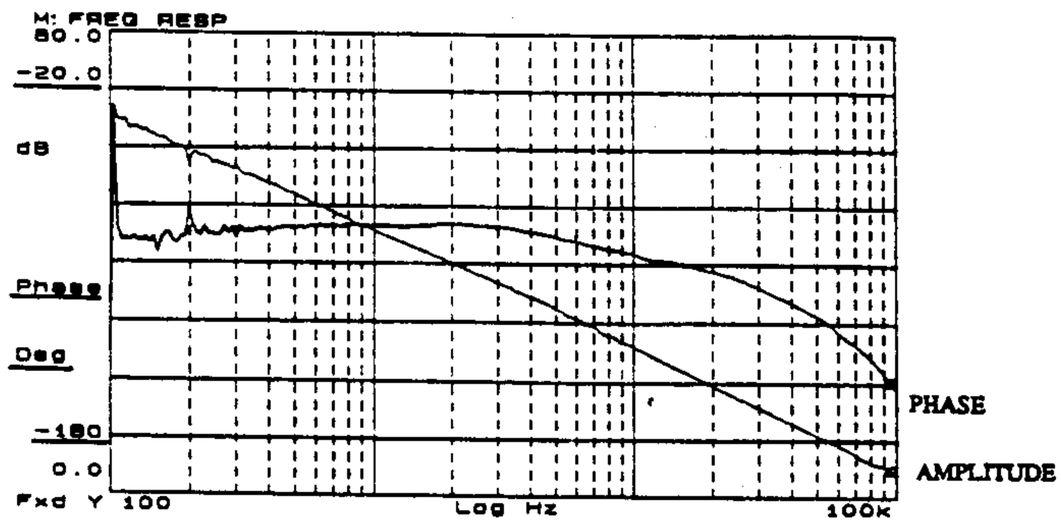

Figure 2. Accumulator RF System: the RF Amplitude Loop Frequency Response

3. THE MAIN RINGS RF SYSTEM

One RF cavity will be installed on each intersecting storage ring. The resonators, made of OFHC copper, are equipped with high order mode (HOM) suppressors. The RF power source consists of a 150 kW/CW klystron amplifier; a high power ferrite circulator is used to protect the klystron when high standing wave regime occurs. The parameters of the main RF system, for 30 bunches operation, are shown in Table II.

Table II
The Main Ring RF Parameters with 30 Bunches

RF Frequency	368.25 MHz
Harmonic Number	120
Cavity Impedance ($V^2/2P$)	2.40 MΩ
Cavity Q_o (with WGs)	40000
RF Peak Voltage	260 kV
Cavity Power	15 kW
Beam Current	1.41 A
Beam Power (with Parasitic Losses)	28 kW
Klystron Power	150 kW

3.1 The DAΦNE RF Cavity

The design of the RF cavity has been conceived with the aim of reducing the coupling of the HOMs to the beam spectrum lines [4]. The cavity is connected to the beam pipe with large and long tapered tubes which yield a significant reduction of the HOM R/Q impedances. Moreover, three waveguides with cut-off above the fundamental mode (FM) frequency are incorporated in the resonator to convey the beam induced HOM energy out and to dissipate it on an external 50 Ω load. This is accomplished by means of broadband (0.5÷3 GHz) waveguide to coaxial transitions (BTHD) which have been developed at LNF [5] to this purpose. The damping system, which also includes two additional 1.1÷3GHz BTHDs connected to the tapered tubes, has been tested on a cavity prototype and the measured HOM Qs are listed in Table III. They are below the calculated Q values [6] required to initially operate the machine with 30 bunches together with a bunch-to-bunch digital feedback system. The WG damping system yields a reduction of the FM frequency and Q of about 2% and 12% respectively.

Table III
The Cavity Prototype HOM Quality Factors

F (MHz)	R/Q (Ω)	Unload. Q	Loaded Q	Target Q
745.7	16	24000	70	85
796.8	0.5	40000	210	2500
1023.6	0.9	28000	90	300
1121.1	0.3	12000	300	3500
1175.9	0.6	5000	90	1650
1201.5	0.2	9000	180	4300
1369.0	2.0	5000	170	450
1431.7	1.0	4000	550	870
490.0 °	5.1 *	30500	150	9200
491.3 °	5.1 *	28500	830	9200
523.5 °	14.0 *	31500	150	6200
549.7 °	14.0 *	3200	50	6200

° Dipoles -
* Normalized Impedance -

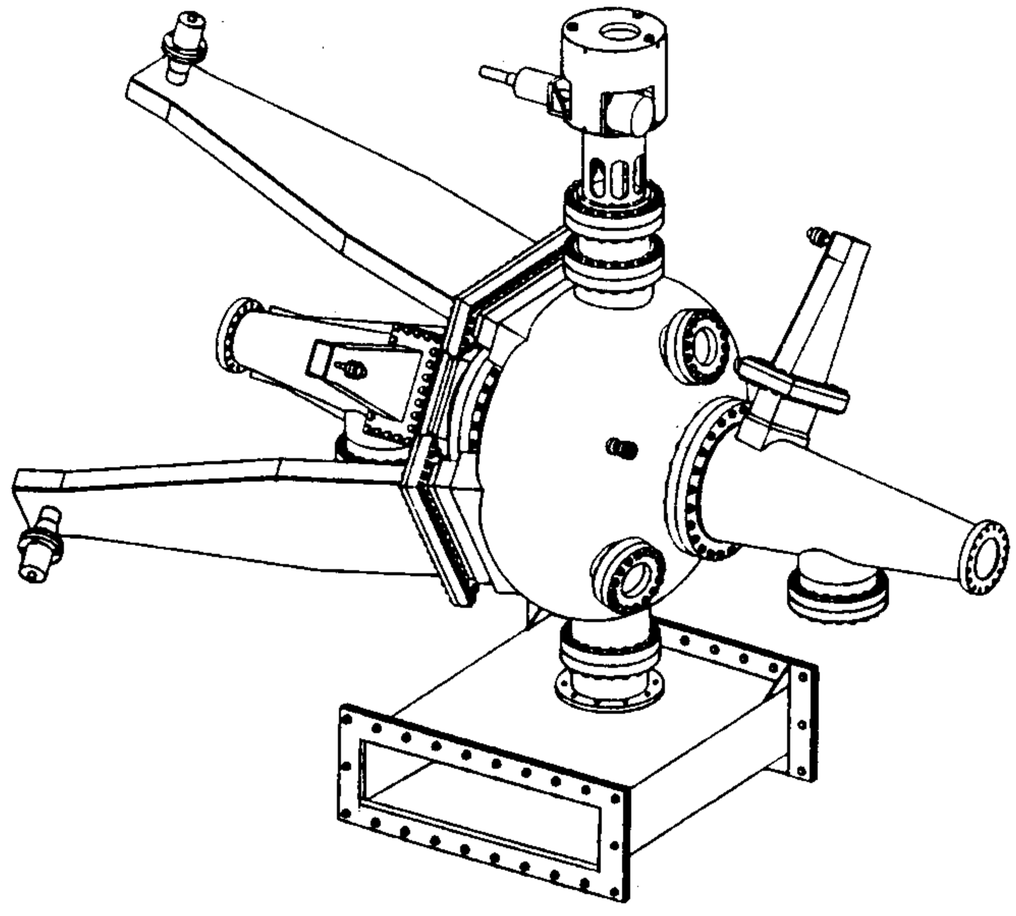

Figure 3. Skecth of the DAΦNE RF Cavity.

A sketch of the DAΦNE cavity is shown in Figure 3. It includes the tuning system (upper cavity side) and the fundamental mode RF coupler (lower cavity side) whose design derives from that of the copper LEP cavities. The BTHD transitions have been successfully power tested as reported in [7]. The first main ring cavity is being fabricated by industry (ZANON, Schio, Vicenza, Italy).

3.2 The RF Power Source

The RF power source of each main ring RF system is a 150 kW/CW klystron operating at 368.25 MHz. The power to be delivered to the beam was estimated in the order of 100 kW at full beam current of 5 Amps. The new klystron TH2145 has been developed by Thomson Tube Electronique and successfully factory tested at full power.

The klystron group delay, i.e. the derivative of the output phase with respect to the angular frequency, should be kept as low as possible at the operating frequency to improve the performances of an RF feedback loop to be closed around the cavity and klystron to provide beam stability under intense beam loading conditions. The RF feedback has been proposed and positively operated in other accelerators [8,9]. A group delay of about 160 nsec has been measured in both DAΦNE klystrons. In order not to increase the group delay further, the klystrons will be positioned at short distance from the cavities (about 7 meters) in the main rings hall. The frequency and group delay responses of the klystron are shown in Figure 4.

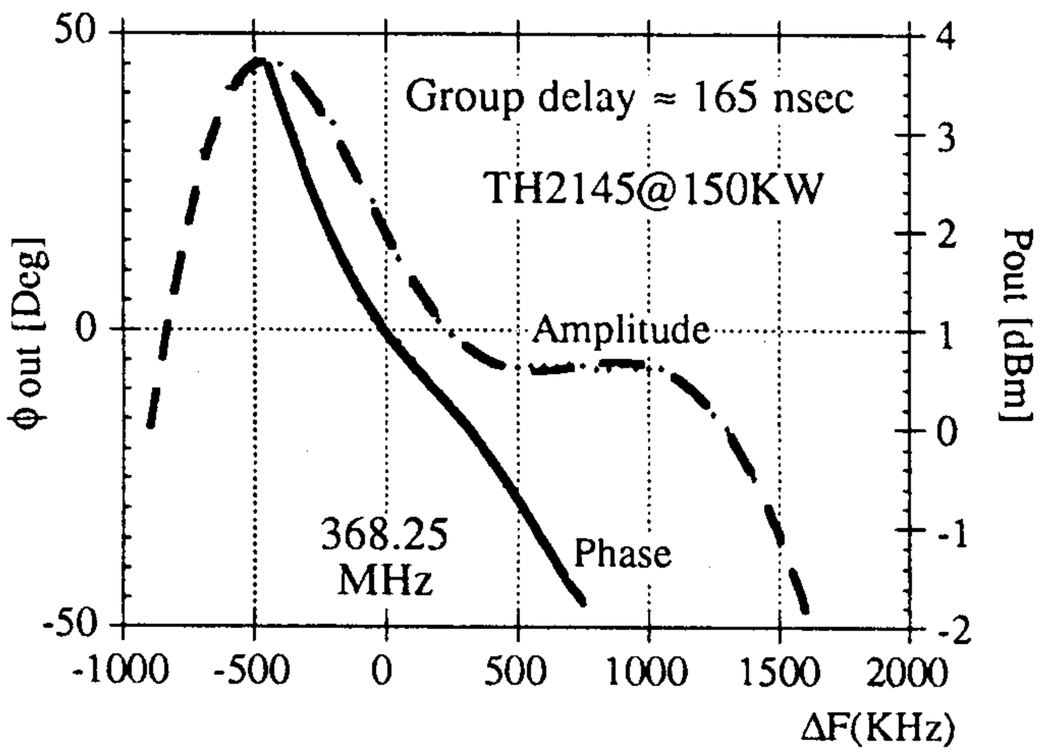

Figure 4. The Klystron TH2145 response

3.3 The Main Ring RF Feedback

To compensate for beam loading when operating the main rings at high current, an RF feedback around cavity and klystron must be implemented, otherwise the longitudinal motion of the beam can become unstable in the Robinson zero frequency mode.

A sample of the cavity RF voltage is fed to the klystron driver back and added with a proper phase to the main RF signal to get a negative feedback connection which reduces the complex impedance seen by the beam according to the following expression:

$$Z'(j\omega) = \frac{Z(j\omega)}{1+G(j\omega)Z(j\omega)} \qquad (1)$$

where $G(j\omega)$ is the feedback gain.

The reduction of the complex impedance allows to increase the instability threshold derived by Robinson [10] and, hence, the maximum storable beam current I_M, according to:

$$1 - \frac{2I_M Z(j\omega)}{V_C|\sin\phi_S|} = 0 \qquad (2)$$

where V_C is the cavity voltage and ϕ_S the synchronous phase. The maximum attainable feedback loop gain, as derived by Boussard, is limited by the group delay of the loop itself where the largest contribution is due to the klystron. In our case, a total delay of about 250 nsec, including the delay of the connecting cables, allows increasing the RF feedback gain as much as we need to reach stable operation even at full beam [11].

5. ACKNOWLEDGMENTS

We are grateful to Mr. Michele Scampati, Alfredo Sprecacenere and Tullio Tranquilli for their continuous enthusiastic support.

6. REFERENCES

[1] The DAΦNE Project Team, "DAΦNE: The Frascati Φ-Factory", in Particle Accelerator Conference, Washington DC, USA, May 1993, p. 1993.

[2] K. Whitham et al., "Design of the e+/e- Frascati Linear Accelerator for DAΦNE", in Particle Accelerator Conference, Washington DC, USA, May 1993, p.611.

[3] S. Bartalucci et al., "Design Criteria and Measurements of the Prototype of the DAΦNE Accumulator Cavity", in 3rd European Particle Accelerator Conference, Berlin, Germany, March 1992, p.1260.

[4] S. Bartalucci et al., "The RF cavity for DAΦNE", in Particle Accelerator Conference, Washington, DC, March 1993, p.778.

[5] R. Boni et al., "A Broadband Waveguide to Coaxial Transition for HOM Damping in Particle Accelerator RF Cavities", LNF 93/075(P), 1993.

[6] S. Bartalucci et al., "Analysis of Methods for Controlling Multibunch Instabilities in DAΦNE", LNF 93/067(P), 1993.

[7] R. Boni et al., "Update on the Broadband Waveguide to 50 Ω Coaxial Transitions for Parasitic Mode Damping in the DAΦNE RF Cavities", this Conference.

[8] D. Boussard, "Design of a Ring RF System", CERN SL/91-2 (RFS), 1991.

[9] P. Krejcik et al., "RF Feedback for Beam Loading Compensation in the SLC Damping Rings", SLAC-Pub-6231, 1993.

[10] K.W. Robinson, "The Stability of Radiofrequency Systems", CEA Report N° CEAL-1010, 1964.

[11] A. Gallo, "A RF Feedback for DAΦNE", DAΦNE Internal Note, RF-6, May 1992.

Update on the Broadband Waveguide to 50 Ω Coaxial Transition for Parasitic Mode Damping in the DAΦNE RF Cavities

R. Boni, A. Gallo, G. Gemme+, F. Marcellini, R. Parodi+, P. Baldini, F. Lucibello, S. Quaglia
INFN Laboratori Nazionali di Frascati, C.P. 13, 00044 Frascati, Rome (Italy)
+INFN Sezione di Genova, Via Dodecaneso 33, 16146 Genoa (Italy)

Abstract

A novel device has been conceived to allow the dissipation of the parasitic mode beam power of the DAΦNE RF cavities on a broadband coaxial 50 Ω load. This avoids the use of RF lossy materials in the waveguides in ultra vacuum. This paper summarizes the project criteria and the experimental tests performed on prototypes made of Aluminum. Furthermore, up-to-date results at high power in under vacuum copper models are reported.

1. INTRODUCTION

The Φ-Factory DAΦNE [1] is under construction at the INFN, Laboratori Nazionali di Frascati. It is a multibunch double ring collider providing e^+/e^- 1020 MeV center of mass collisions at a maximum repetition rate of 368.25 MHz with 47 mA per bunch.

An inherent drawback of multibunch operation of a storage ring is the coupled bunch instability that can arise from the interaction of the particles with the high order modes (HOM) induced in the RF cavities by the preceding bunches. Damping the HOMs of the accelerating cavities is considered the most powerful remedy to this problem; different techniques have been developed depending upon the type of cavity (i.e. normal or superconducting) and the accelerator requirements.

In normal conducting cavities, rectangular waveguides (WG) can be directly applied onto the resonator to extract the HOM energy and dissipate it on matched loads. As an R&D for the DAΦNE project we have tested [2,3] a single cell cavity prototype equipped with three rectangular WGs with cut-off at 492 MHz. The position of the WGs has been chosen in order to have the best coupling with the highest impedance HOMs, like TM011. The HOM energy propagates along the WGs in the TE10 fundamental mode (FM) and must be dissipated on matched loads placed at the opposite side of the WG itself.

2. THE HOM ABSORBERS

The HOM energy coupled out of the cavity must be absorbed by matched loads to reduce the decay time of the parasitic modes (i.e. their quality factor Q). Several kinds of HOM loads have been studied and are being used elsewhere. An overview of the R&D in this field is reported in [4].

In DAΦNE we have chosen a different way of damping the HOMs. The propagating mode of the HOM beam power is converted from the WG TE10 to a coaxial TEM by means of a broadband transition which allows to dissipate the energy on an external commercial 50 Ω load through a ceramic vacuum window of standard design. It is possible, in this way, to sample the HOM power with a directional coupler.

The study and the experimental work which led to the development of the broadband transition is widely reported in another paper [5]. In this report we summarize the concepts which the transition is based on and report updated information and experimental results.

2.1 The Waveguide to Coaxial Line Transition

A broadband waveguide to coaxial transition for HOM damping (BTHD) in particle accelerators has been studied and proposed for the use in the DAΦNE RF cavities.

The BTHD essentially consists, as sketched in Fig. 1, in a tapered 50 cm long WG connected to a mode transducer from the WG TE10 to the TEM of a 7/8" 50 Ω coaxial line. The taper transforms the 305 x 40 mm^2 rectangular WG cross section at the cavity side into a 140 x 40 mm^2 double ridge WG section with 63 x 17 mm^2 ridges. This tranformation is necessary to increase the ratio of the cut-off frequencies TE30/TE10 and, hence, to increase the BTHD bandwidth.

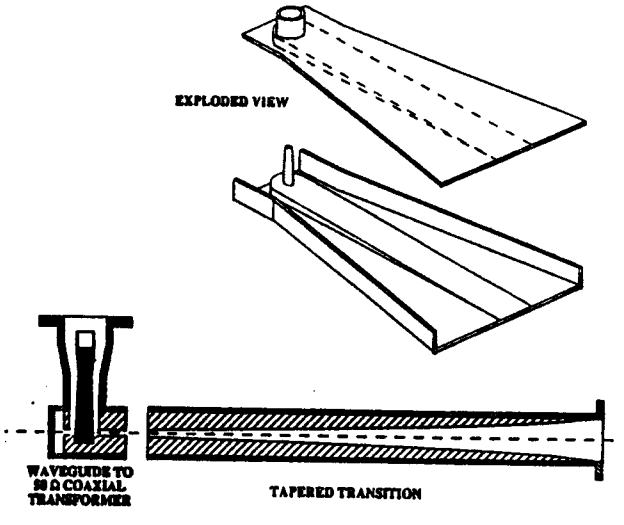

Figure 1. Sketch of the BTHD Broadband Transition.

The BTHD design has been first studied analytically following the indications of the existing technical literature [6,7]. Then the project has been refined with a step-by-step procedure with the 3D Hewlett Packard computer code HFSS [8]. The longitudinal profile of the ridges is of exponential type and has been calculated in order to keep the TE10 cut-off frequency of the tapered WG within ± 2 MHz around the nominal value. This yields a smooth variation of the characteristic impedance along the tapered WG and therefore a better frequency response in the full bandwidth is obtained. The mode transducer has been also designed by means of HFSS with a "cut and try" procedure. The length of the shorted WG section behind the inner coaxial (also called "back cavity") must be experimentally adjusted to optimize the frequency response of the BTHD. The ridge gap at the coaxial output position is 6 mm. The output ceramic feedthrough is a 7/8" coaxial which can safely handle the parasitic beam power that has been estimated below 1 kW per WG. Three Aluminum BTHD prototypes have been built and low power tested. Figure 2 shows an open view of a BTHD model and Fig. 3 gives the measured S11 parameter vs frequency.

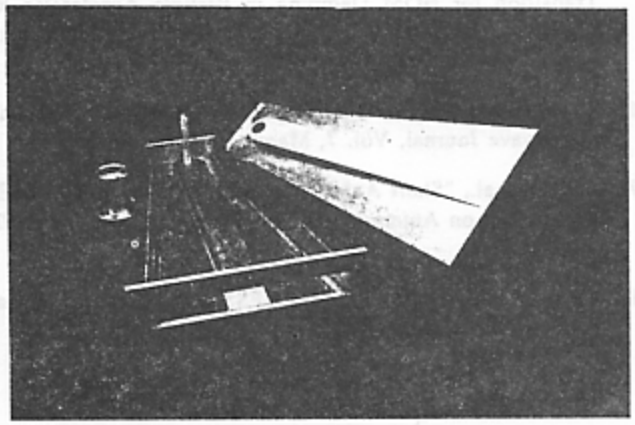

Figure 2. The BTHD Prototype: the open view.

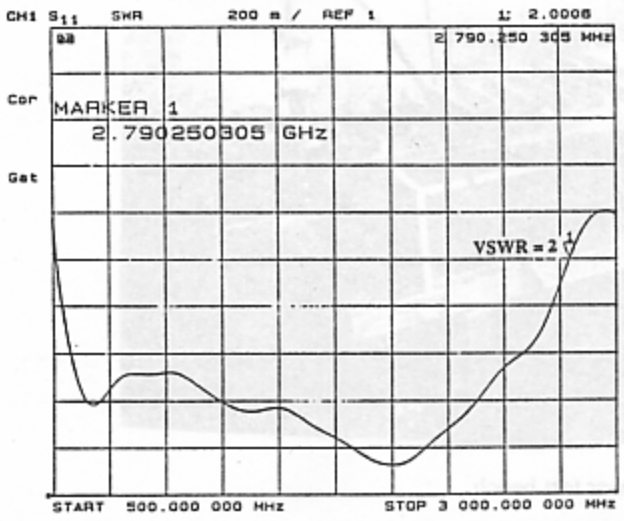

Figure 3. The BTHD response: VSWR vs Frequency.

The VSWR of the Aluminum BTHDs is below 2 in the range 500 ÷ 2800 MHz; therefore, they have been incorporated in the cavity prototype and the HOM damping has been measured [5]. The result has been considered satisfactory enough to proceed with the construction of a model to be tested in vacuum at high power.

2.2 The BTHD Copper Model

In order to check the capability of the transitions to operate reliably at high RF power in ultra high vacuum (UHV), three oxygen free high conductivity (OFHC) copper BTHDs have been fabricated. All the joints have been brazed under vacuum at 900 °C at INFN Legnaro National Lab. A water cooled straight 30 cm rectangular WG has been added to the BTHD to avoid excessive penetration of the cavity FM into the transition. The FM dissipation in the WGs has been estimated ≈ 1 kW per WG. The BTHD external structure has been also mechanically reinforced to reduce the stress due to the atmospheric pressure when operating in UHV. One copper transition is depicted in Fig. 4. The flanges vacuum tightness is obtained with Helicoflex gaskets. The RF contacts are ensured by Silver plated Be-Cu springs on both rectangular and circular 7/8" flanges and with Silver plated La-Cu sliding contacts on the back cavity port.

Figure 4. The OFHC Copper BTHD.

2.3 The ceramic vacuum feedthrough

A 50 Ω coaxial ceramic window has been designed to carry the HOM power out of the BTHD and feed an external load. The 7/8" standard has been considered sufficiently safe to withstand 1 kW CW RF power.

The feedthrough has been also studied with the HFSS code. The goal was to design a device with the widest possible frequency bandwidth. The project is outlined in Fig. 5.

A 5 mm thick Al_2O_3 disk, to be brazed to the inner/outer conductors, ensures the vacuum tightness. In addition, a 5 mm thick Macor disk is placed onto the air side of the Al_2O_3 disk. This allows to have more gradual variations of the dielectric constant. In this way, the feedthrough frequency response is excellent, being the simulated VSWR lower than 1.2 in the full range 500 ÷ 3000 MHz. The ceramic window is being manufactured by the French company Ceramex.

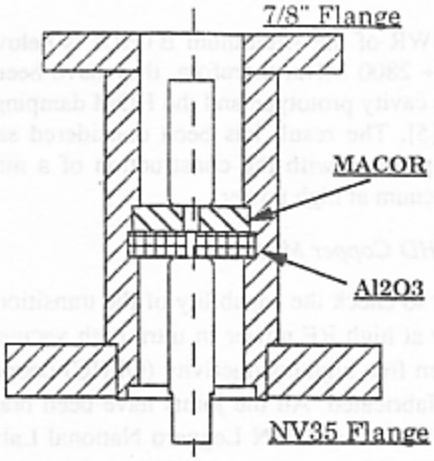

Figure 5. Sketch of the coaxial ceramic window.

2.4 The BTHD Power Tests

Two Copper BTHDs have been RF power tested in UHV. They were connected through the rectangular flanges by means of an intermediate stainless steel WG section which is needed to house the pumping ports and the vacuum gauge. The test bench is shown in Fig 6. Two 7/8" coaxial vacuum connectors of 1.5 GHz bandwidth, already available in the Laboratory have been used for the connection to a TV tetrode amplifier and to a 50 Ω load. The BTHDs have been tested at 740 MHz, close to the TM011 frequency, at a power level of 1 kW/CW which is the maximum estimated HOM power extracted from the cavity in 30 bunches operation. The test has been performed at $2 \cdot 10^{-9}$ Torr which is the DAΦNE nominal UHV. Although no Titanium coating was provided inside BTHD, no multipactoring discharges occurred at any power level up to 1 kW.

4. ACKNOWLEDGMENTS

The authors acknowledge the invaluable support to this work of Dr. Virgilio Chimenti, Dr. Alberto Clozza and Mr. Gianfranco Serafini for their cooperation to this work.

5. REFERENCES

[1] The DAΦNE Project Team, "DAΦNE: The Frascati Φ-Factory", in Particle Accelerator Conference, Washington DC, USA, May 1993, p. 1993.

[2] S. Bartalucci et al., "The RF Cavity for DAΦNE", in Particle Accelerator Conference, Washington DC, May 1993, p. 778.

[3] S. Bartalucci et al., "Analysis of Methods for Controlling Multibunch Instabilities in DAΦNE", LNF 93/067(P), 1993.

[4] I. Campisi, "The Workshop on Microwave-Absorbing Materials for Accelerators", in Particle Accelerator Conference, Washington DC, May 1993, p. 1115.

[5] R. Boni et al., "A Broadband Waveguide to Coaxial Transition for HOM Damping in Particle Accelerator RF Cavities", LNF 93/075(P), 1993, (to be published on Particle Accelerators)

[6] K. Walton et al., "Broadband Ridged Horn Design", Microwave Journal, Vol. 7, March 1964, pp. 96-101.

[7] J. Kerr et al., "Short Axial Length Broadband Horns", IEEE Transaction on Antennas and Propagation, September 1973, pp. 710-714.

[8] Hewlett Packard Company, "HFSS: the High Frequency Structure Simulator", trademark.

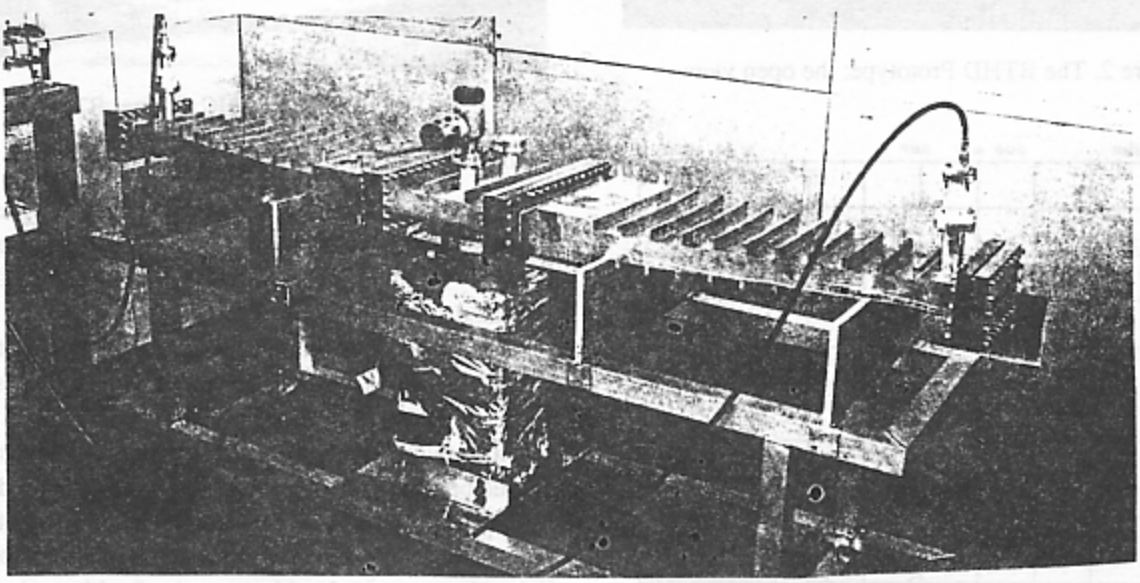

Figure 6. The BTHD power test bench.

The Interaction Region Vacuum Chamber for the KLOE Experiment

A. Clozza, G. Raffone
INFN LNF
C.P. 13, 00044 Frascati (Roma)
Italy

Abstract

A vacuum and supporting system for the interaction region of the KLOE experiment, that will be installed on the DAΦNE Φ factory in Frascati (Italy), have been designed. A short description of the vacuum system and of the supporting system for the vacuum chamber will be presented on this paper.

1. INTRODUCTION

KLOE is a general purpose detector, see figure 1, that will be installed on DAΦNE the Frascati Φ factory. This detector is optimized for the study of CP violation in K^0 decays with the aim of achieving a statistical accuracy of $\sim 10^{-4}$ in one year run at the DAΦNE target luminosity of $\sim 10^{33}$ $cm^{-2}s^{-1}$.

The vacuum chamber, for the KLOE experiment interaction region, has been designed taking into account several stringent requirements needed to fulfill the operating condition of the detector itself. Some of the requirements are: mean vacuum pressure level better than $1 \cdot 10^{-9}$ torr, vacuum chamber around the interaction point as transparent as possible to the produced particles, all the components of the support, the quadrupole magnets and any other thing, that can interact with the produced particles, must stay within a maximum detector acceptance angle of 9 degrees respect to the beam axis.

2. VACUUM SYSTEM

2.1 Vacuum chamber

It is possible to divide the vacuum pipe in three main sections. The first one between the first separator magnet and the first low-β quadrupoles triplet, the second one between the first and the second low-β quadrupole triplets and the third one between the second low-β quadrupole triplet and the second separator magnet.

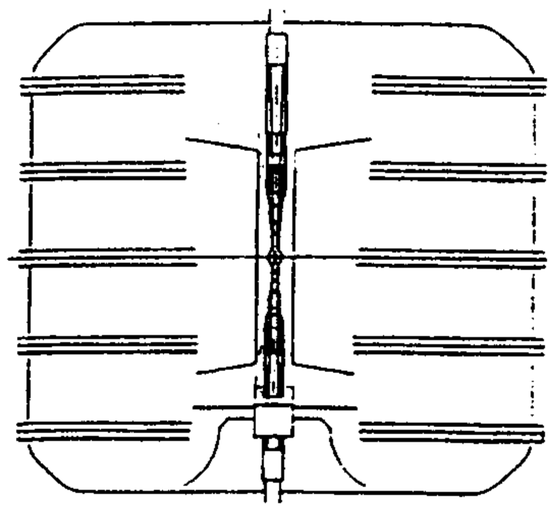

Figure 1. View of the KLOE detector

The first and the third section of the vacuum chamber are equal and are made of AISI 304 L stainless steel (2 mm thickness) with a copper coating inside in order to reduce the ohmic current losses.

2.2 Beryllium Vacuum Chamber

The second section is made of pure beryllium (0.5 mm thickness) to provide a very good transparency in terms of radiation length and scattering angle. See figure 2.

The beryllium I.R. beam pipe is about 0.7 m long and the cross section diameter grows up from 86 mm to 200 mm at the interaction point.

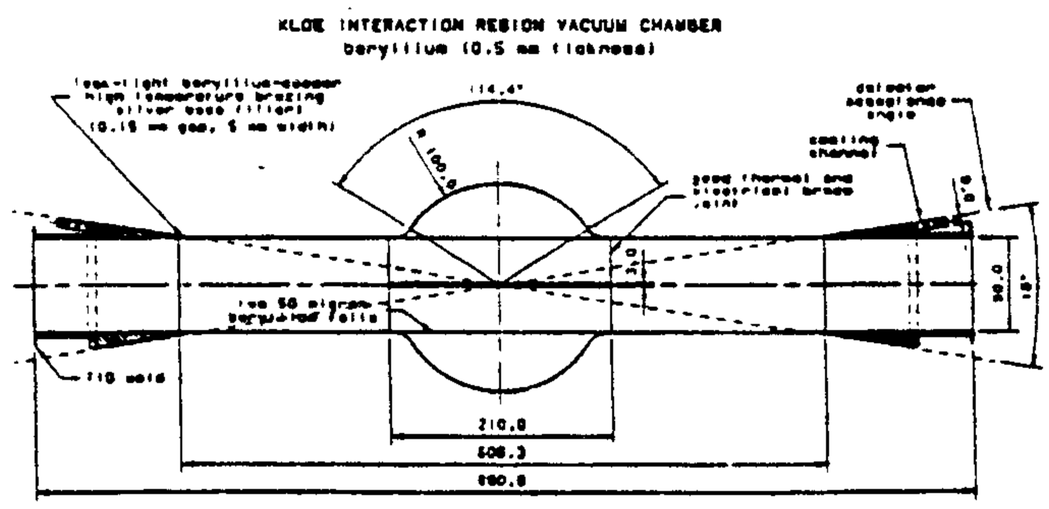

Figure 2. The KLOE beryllium vacuum chamber

The middle bulb-shaped part of the chamber makes the manufacturing difficult from several points of view: machining, brazing techniques, tight tolerances and cleaning conditions. Some brazing techniques are still under development.

The beryllium chamber is directly brazed onto the stainless steel pipe; the total length of the part of the pipe inside the detector is about 4 m and requires four simply support points.

Water pipes, brazed as close as possible to the interaction point, provide the cooling needed to compensate for the RF thermal load on the vacuum chamber.

Inside the spherical part of the chamber there is a 50 micron beryllium shield (180 mm long) to reduce RF wall losses and beam instability.

This shield is brazed at both ends in order to have a good thermal and electrical continuity. Under the thermal load the shield buckles into different shapes depending upon the initial curvatures of its surface.

When the shield is made of several circumferential strips, it is possible to shows clearly that an outward curvature of the strip often does not avoid the anti symmetric mode of buckling; furthermore the double curvature surface of the strip leads to a torsional out of plane mode of buckling.

2.3 Pumping System

The vacuum requirements for the KLOE interaction region brought us to a special design for the pumping system.

Table 1 shows the main vacuum related parameter for the interaction region. The value of the gas load has been evaluated using for the desorption coefficient η the mean value of $1 \cdot 10^{-6}$ molec/photon. Although the gas load is not very high, the geometry of the vacuum chamber and the requirements for the detector make things harder. In our case, indeed, the vacuum chamber is essentially a long narrow pipe.

Table 1
Vacuum related parameters

Total photon flux	$3 \cdot 10^{19}$ phot./s
Total gas load	$9 \cdot 10^{-7}$ torr l/s
Total power load	180 W
Max. mean pressure	$5 \cdot 10^{-10}$ torr

The main problem to solve, designing a pumping system for a long pipe with a distributed gas load, shown in figure 3, is to have a pressure distribution, along the pipe, as uniform as possible. The simplest solution is a pumping system which pumps are placed at regular distance along the pipe.

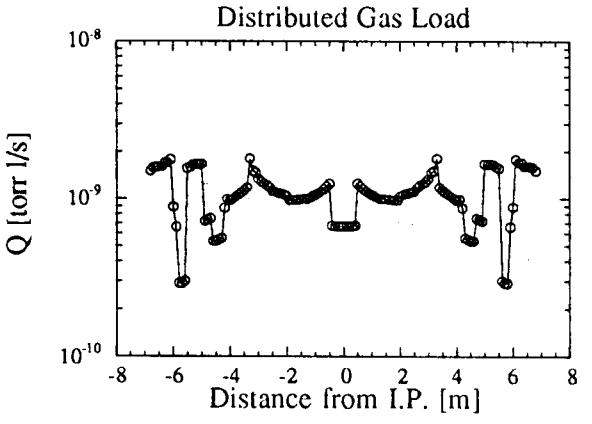

Figure 3. Gas load distribution along the vacuum chamber.

The solution we adopted is a compromise between the uniform distribution of the pumping elements and the mechanical constrains of the detector and of the vacuum pipe itself. Figure 4 shows the pumps arrangement we have chosen for the interaction region. This pumping system is a combination of lumped sputter ion pumps, distributed sputter ion pumps and non evaporable getter pumps. In figure 4 it is possible to see the location of the various pumps: a pair of 230 l/s lumped sputter ion pumps is placed after each splitter magnet, a 200 l/s distributed sputter ion pump is placed inside each splitter magnet, a 500 l/s distributed sputter ion pump is placed inside each compensator magnet, and a 800 l/s non evaporable getter pump is placed between each compensator magnet and the KLOE solenoid. There are no pumps inside the detector near the interaction point.

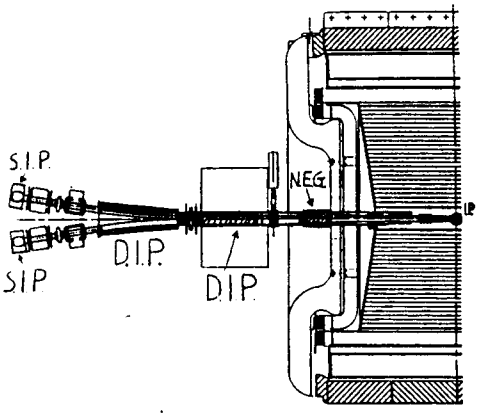

Figure 4. Pumping system arrangement

Lumped sputter ion pumps are simply available on the market. On the contrary, for distributed sputter ion pumps and non evaporable getter pumps we did an R&D work whose results are described below.

For the distributed ion pump placed inside the splitter magnet, where the magnetic field strength is about 1.7 kG, like in a commercial pump, we will use a pumping element with the same cell dimensions of a standard diode ion pump. In the compensator magnets, where the magnetic field strength is about 1.5 T, we will use a special pumping element, which cell dimensions are shown in table 2.

Table 2
Pumping element dimensions

Cell diameter	10 mm
Cell length	20 mm
Anode-cathode gap	5 mm

With a prototype of this pump (anode composed by 100 cells) we have measured a pumping speed of 50 l/s at $1 \cdot 10^{-9}$ torr, this means that the pumping speed for the single cell is 0.5 l/s. In the compensator magnets there is sufficient room to obtain about 500 l/s of pumping speed with this kind of pump.

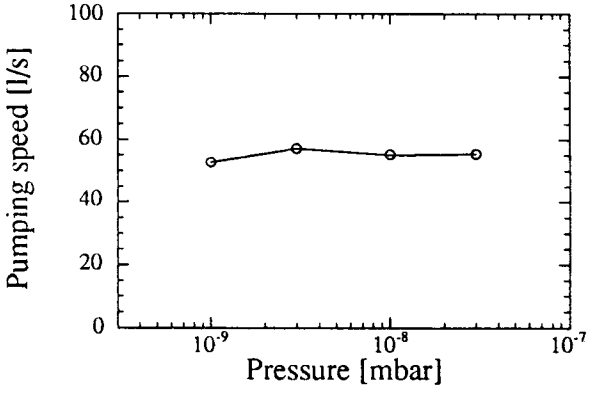

Figure 5. Pumping speed of the prototype of the distributed sputter ion pump working at 1 T.

The decision to use a Non Evaporable Getter pump arises from the development of a new kind of getter from SAES Getters.

A preliminary design, done in collaboration with SAES Getters, foresees a pump composed by 480 blades, which initial pumping speed is of the order of 2000 l/s, for CO, and decreases to about 800 l/s after having pumped about 50 torr liters of gas, this means about 2 years of full current 24 hours a day machine operation.

2.4 Pressure Profile

The vacuum system designed for the interaction region is able to reach a mean pressure of about $3.2 \cdot 10^{-9}$ torr after 100 Ah of stored beam, the mean pressure falls down to $9 \cdot 10^{-10}$ torr after 1000 Ah and to $4 \cdot 10^{-10}$ torr after 5000 Ah.

The maximum value of the pressure with the proposed configuration of pumps is $8 \cdot 10^{-9}$ torr after 100 Ah of stored beam, and is determined by the conductance of the vacuum pipe between the NEG pumps and the Interaction Point.

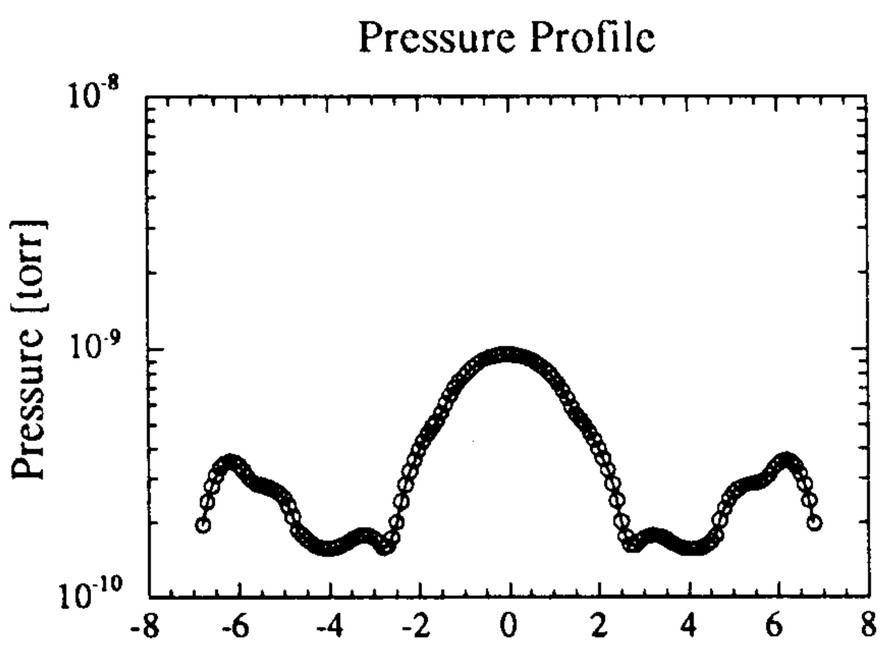

Figure 6. Pressure profile at full conditioning

3. SUPPORTING SYSTEM

The supporting system consists mainly into two independent structures: the vertex detector support and the triplet assembly support.

The basic idea is to have two independent supports to allow relative motions between them during the mechanical alignment of the permanent magnet quadrupoles.

The vertex support is made of carbon fiber composite material; it is a simple cylindrical structure (light and rigid) about 4 m long and supported at the end cones of the tracker chamber. There is a small gap between the vertex support and the tracker inner wall (500 mm diameter) to house a proper tooling device during the installation.

As before pointed out, the vacuum pipe needs four simply support points to avoid both high bending stresses and the Brazier's effect.

These support points are more or less equally spaced along the vertex support; two of them are collars rigidly joined to the end plates of the vertex detector; the other two are located at the end of the vertex support (i.e. close to the end cones of the tracker). Then a compact structure involving both the vertex detector and the beam pipe is obtained.

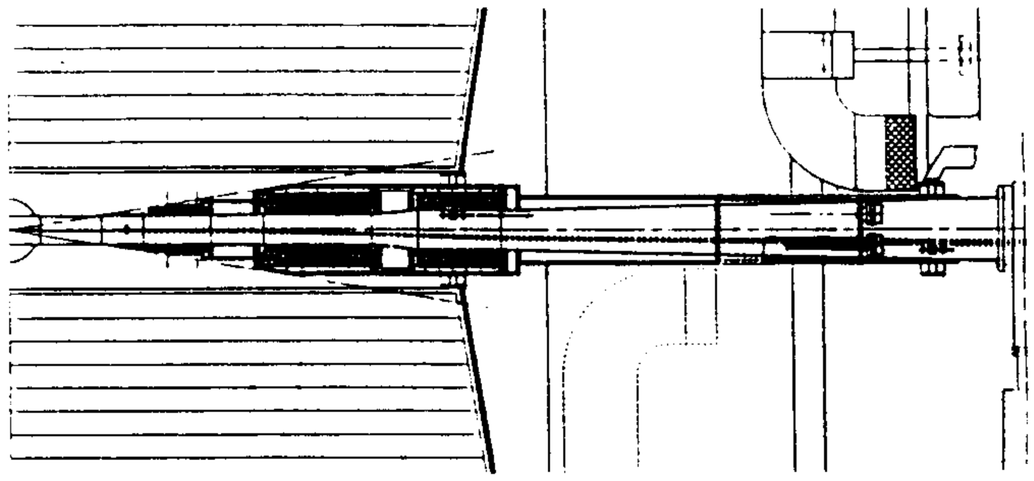

Figure 7. Supporting system layout

The triplet support allows a remote control of five of its degrees of freedom (vertical and horizontal positions, roll, pitch and yaw angles) by means of a five cams system; this support will be able also to carry an additional calorimeter besides the low-β permanent magnets.

The main part of this support will be made of a carbon fiber in order both to minimize the amount of material inside the detector and to obtain an acceptable bending at its end.

It will be simply supported in two sections: the latter inside the detector, right on the end of the tracker cone, and the former outside close to the compensator solenoid.

This support must be splitted longitudinally to allow the beam pipe and the permanent magnets installation.

4. CONCLUSIONS

The vacuum and supporting system for the interaction region of the KLOE experiment has been designed to meet the requirements needed to fulfill the operating condition of the detector itself.

The vacuum chamber has a structure, 2 mm thick stainless steel and 0.5 mm beryllium, enough rigid, that could be self supporting, and at the same time it provides a very good transparency, 0.5 mm beryllium, in therms of radiation length and scattering angle.

The pumping system is able to reach a mean pressure of about $5 \cdot 10^{-10}$ torr at full current, 5 A of stored current for each beam, after a reasonable conditioning of the order of 2 or 3 months.

The supporting system, made of carbon fiber composite material, consists mainly into two independent structures to allow relative motions between the vertex detector and the triplet assembly during the mechanical alignment of the permanent magnets. The vertex detector supporting structure will hold also the vacuum chamber.

High Current Density Septum Prototype for Accumulator and Storage Rings of DAΦNE, the Frascati Φ-Factory

M. Modena, H. Hsieh and C. Sanelli
INFN Laboratori Nazionali di Frascati, C.P. 13 - 00044 Frascati (Roma) - Italy

Abstract

DAΦNE is a Φ-factory, presently under construction at INFN, Laboratori Nazionali di Frascati. The injection/extraction magnetic system for both the accumulator and storage rings, composed of two septa, has been designed and is now under construction. A full size prototype of the 38 mrad thin septum near the machine has been built and completely tested at LNF. This septum is of high current density and edge cooled type. This paper describes the mechanical design and the results of the magnetic measurements in comparison with the FEM calculations.

1. INTRODUCTION

A 510 MeV electron/positron colliding facility known as DAΦNE [1], is currently under construction at INFN's Frascati National Laboratory.

The project consists of two storage rings and an energy injector system. Electrons and positrons will be injected into the DC accumulator alternatively from Linac at a frequency of 50 Hz. The storage rings will only have injection frequency of few Hz.

Figure 1 depicts the physical layout of the system. Injection/extraction of electrons and positrons is accomplished by two DC Septa [2].

The "thin" septum is a 38 mrad high current density, edge cooled type. Due to the fact that this element is the most critical one of the injection system, a full size prototype was built at Frascati Labs, in order to evaluate the magnetic and thermal characteristics.

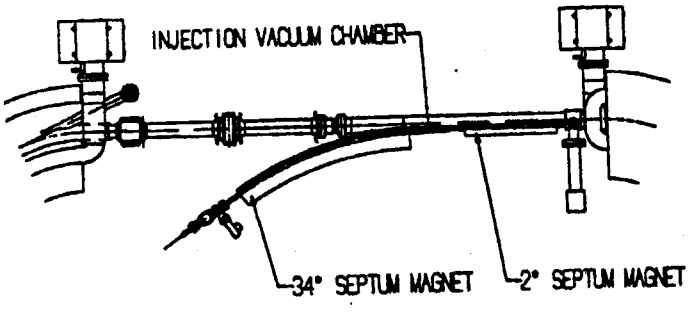

Figure 1. Injection/extraction Septum System

2. SEPTUM DESIGN

2.1. Septum Design

Figure 2 shows the cross section of the septum. The principal design constraint was the allowable maximum septum thickness set by machine physics group in the order of 4 mm. It of course includes the thickness of two vacuum chambers, reducing the thickness of the current carrying conductor to 1.5 mm. The resulting current density is in the order of 60 ampere per square mm. The septum coil is electroformed on two thin wall, rectangular tubings, to form an intimate thermal contact between conductor and cooling tubes for proper heat transfer. These tubings are of stainless steel AISI 304 L to avoid excessive current sharing with the conductor. The back coil is of conventional copper hollow conductor.

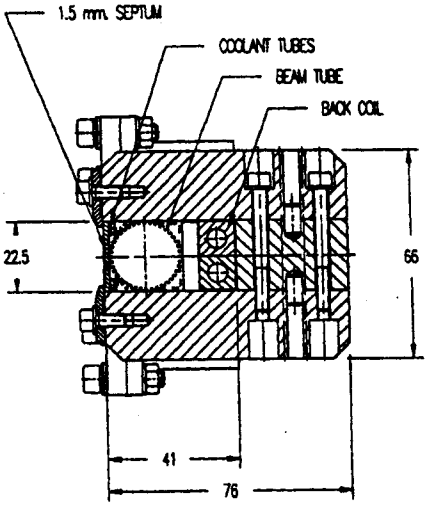

Figure 2. Septum Section

All the electrical insulation will be provided with 130 μm thick pressure sensitive Kapton tape. The additional function of the Kapton tape, due to its extreme low thermal conductivity, is to insulate thermally the beam chamber from high temperature septum, this will prevent the thermal outgassing of the stainless steel septum beam tube, so near to the machine that it is considered as part of the machine vacuum system. The iron yoke is of low carbon Armco steel type, it is detachable so that the septum can be installed or removed from its location easily. Table 1 shows some of the more relevant parameters of this septum.

Table 1. Septum Parameter List

Field	0.104	T
Bend Angle	38	mrad
Gap Height	22.5	mm
Magnetic Length	623	mm
Septum Cond. Area	33.75	mm^2
Current	2125	A
Current Density	63	A/mm^2
Resistance	0.33	mΩ
Power	1.49	kW
Voltage	0.7	V
N. of Water Circuit	1	
Water Flow Rate	0.1	L/s
Water Pressure Drop	3	Atm
Water Temp. Rise	5	°C

2.2 F.E.M. Analysis

The magnetic design has been carried out with POISSON code (2-D), taking into account the real current distribution within the septum and coolant tubes. Due to the small thickness (0.13 mm) it was impossible to mesh the Kapton electrical insulation. This fact involves that the computed lateral fringing field is surely lower of the real one. One of the aims of the prototype construction was the exact evaluation of the real fringing field that is required to be very low to avoid interference with the stored beams.

The thermal loading of the septum is rather severe due to high current density and edge cooled feature. Thermal analysis has been performed by using ANSYS code, with initial water temperature of 30 °C and assuming constant thermal characteristics of the materials. The computed maximum temperature along the median plane is ≈ 51 °C, there is negligible thermal gradient across the tube wall. Assuming tubings remain rigid, the maximum thermal compressive stress in the copper will be ≈ 440 kg/cm^2, which is below endurance limit of the copper.

3. SEPTUM PROTOTYPE CONSTRUCTION

All parts of the magnet with exception of the septum coil were constructed and assembled at Frascati Labs. The iron was worked with a digital controlled milling machine. The global machining tolerance measured after the iron assembling was less than 0.07 mm. The back coil was obtained starting from a 18x18 mm square holed conductor copper, and all the hydro/electrical connections were obtained from solid copper.

The septum coil was constructed by Tecnol (Florence-Italy) electroforming the copper septum on 2 rectangular pipes (inner dimension: 2x4 mm.) of stainless steel AISI 304 L. For a better fixation of the copper a layer of 10 μm of nickel was deposited on the stainless steel. The max. difference in the electroformed thickness was less than 0.17 mm.

An hydraulic test was performed on the assembled system with a test-pressure of 10 bar. The required water flow rate of 6 l/min. is obtained with a inlet pressure of 5.7 bar.

4. PROTOTYPE MAGNETIC MEASUREMENTS

The magnetic measurements were performed with a Hall Effect Digital Teslameter (from Group 3 - New Zealand) mounted on a X, Y, Z digital moving system (from Micro-controle - France).

The digital moving system permits the probe-keeper to be moved along 3 axes and to be rotated around 2 axes. A granite bench on which the positioning tables are mounted, and a Hewlett-Packard computer HP 9000/300 complete the system. Four of the five movements (X, Y, Z, ϕ) are automatized by means of stepping-motors. The movement resolution is 10 μm. Normally, the movements are remotely controlled by computer, so that dedicated softwares have been written to perform sets of measurements, i.e. the control of sequential steps of the stepping-motors that move the Hall probe along predefined paths. The calibration of the Hall probe is done comparing the instrument with a NMR teslameter (from Metrolab - Switzerland) in a stable and constant external dipole field.

We have done different set of measurements inside the magnet (paths parallel to the magnet axis) and outside in the fringing field region (paths parallel and perpendicular to the magnet axis).

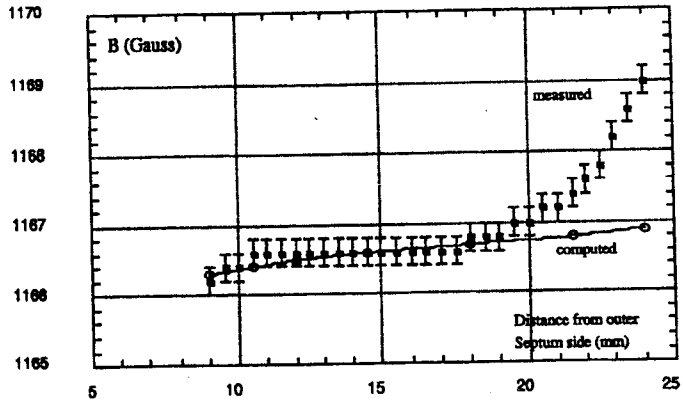

Figure 3. Septum Inner Field

Figure 3 shows the field inside the magnet comparing the measurement to the FEM calculation.

The measurements were done at different sections, showing some differences among different sections. These differences are probably due to the mechanical tolerances of the iron and copper pieces. The agreement between the measured and computed values is very good especially in the left side of the plot (septum coil direction). The discrepancy on the right side (back coil direction) of about 0.1 % is due to the presence of the Kapton insulation between the coils and the iron. The gap of this Kapton layer (0.13 mm), causing degradation of the field quality, was not taken into account in the FEM calculation.

Figure 4 shows the comparison between the measured and computed lateral fringing field.

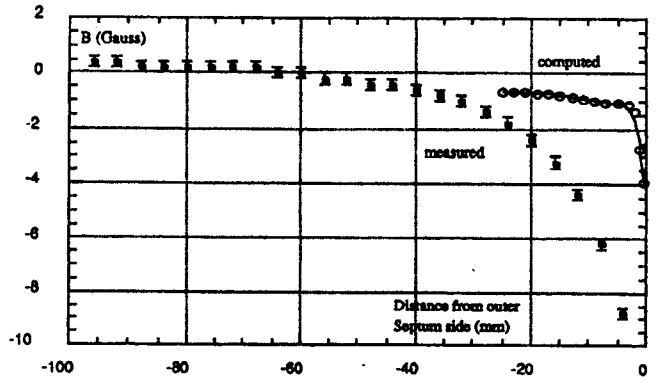

Figure 4. Septum Fringing Field

Also here the discrepancy is caused by the presence of the Kapton insulating tape gap between coil and iron, gap that is not present in the computer simulation. Nevertheless the measured fringing field is very low; less of 2 Gauss at 25 mm from the septum coil.

4. CONCLUSION

A full size 2° septum was built at Frascati Labs. The prototype was fully tested and measured. The results are satisfactory. The thermal loads, critical in these kind of septa, are acceptable. Also the magnetic behaviour (field quality and stray field level) is compatible with the requested one. The components are under series production for the construction of four septa needed for DAΦNE Accelerator Complex.

5. REFERENCES

[1] The DAΦNE Project Team : "DAΦNE Status Report" , paper presented at EPAC 92, 3rd European Particle Accelerator Conference, Technical University of Berlin, Germany, March 24-28, 1992. Proceedings of 3rd European Particle Accelerator Conference, Vol. I p. 60.

[2] M. Modena, H. Hsieh and C. Sanelli: "High Current Density Septa for DAΦNE Accumulator and Storage Rings" EPAC 92, 3rd European Particle Accelerator Conference, Berlin - Germany, March 1992. Proc. p. 1472

The 1.8 Tesla Wiggler for the Main Rings of DAΦNE, the Frascati Φ-Factory

Hank Hsieh, Michele Modena, Miro Andrea Preger, Claudio Sanelli, Sandro Vescovi
INFN, Laboratori Nazionali di Frascati - 00044 Frascati (Roma) - Italy

Abstract

DAΦNE is a Φ-Factory, presently under construction at INFN, Laboratori Nazionali di Frascati. To improve radiation damping and control beam emittance, eight 1.8 Tesla room temperature wiggler magnets will be installed in two main rings. A full size prototype, built by Danfysik (Denmark), has been designed and completely characterized at LNF. This paper describes the mechanical design of the magnet and the magnetic measurements.

Comparison between the measured field and the 3-D FEM code calculations is also presented.

1. INTRODUCTION

DAΦNE, an electron-positron collider [1] working at the Φ resonance energy (510 MeV per beam), is being realized in the INFN Frascati National Laboratory. Commissioning is foreseen in fall 1996.

In order to achieve a luminosity improvement by two orders of magnitude with respect to existing facilities at the same energy, a double ring scheme has been chosen, with up to 120 bunches crossing in two low-β interaction points, where detectors with longitudinal field are installed.

Beam-beam interaction set limits to the maximum achievable luminosity, which are particularly severe at low energy. Experience with existing e^+e^- storage rings [2] and theoretical considerations [3] show that radiation damping is a strong parameter in determining the achievable luminosity. For this reason 4 wigglers have been inserted in each ring, in the center of the achromats, which increase the radiated energy from 4.3 to 9.3 KeV per turn. In addition, by slightly changing the betatron functions in the wigglers, it is possible to tune the beam emittance over a wide range in order to reach the optimum luminosity at any beam current.

Two conditions in the wiggler field must be satisfied to avoid closed orbit distortion: the vertical field integral along the beam trajectory must vanish and the field distribution must be symmetric with respect to the wiggler center. Moreover, it is necessary that the integrated sextupole term, caused by the finite pole width, does not affect the nonlinear motion of the stored particles.

A wiggler prototype built by Danfysik (Denmark) has been delivered in January 1994, and a complete set of electric and hydraulic tests, mechanical and magnetic measurements has been performed, in order to release authorization for series production.

2. MECHANICAL DESIGN

Figure 1 shows a view of the assembled wiggler prototype [4].

The magnet yoke is made of low carbon steel. The final half-pole plates are bolted to the return leg with suitable locating dowels, to allow easy detaching and modification, if required, during magnetic measurements. The width of the wiggler vacuum chamber is ≈50 cm, and due to this large size transverse aluminum ribbings are mandatory both for stress and strain.

In the final configuration these ribbings have a rounded "C" shape, which is different from the original design. The Table 1 recalls the most important parameters of the wiggler design.

Table 1 - Wiggler magnet prototype parameters

Nominal beam energy (MeV)	510
Magnetic field at the gap center (Tesla)	1.8
Wiggler period (mm)	640
Number of periods	3
Amper-turns per pole (A)	56160
Turns per pole	80
Cu cond. cross section (mm * mm)	7 * 7
Cooling hole diameter (mm)	4.0
Nominal Current (A)	702
Maximum Current (A)	750
Current density (A/mm^2)	18.7
Max. Current density (A/mm^2)	20.6
Nominal Voltage (V)	377
Max. Voltage (V)	403
Nominal Power (kW)	265
Max. Power (kW)	302
Water circuits per coil in parallel	5
Total cooling water flow rate (l/min)	146
Water velocity (m/sec)	2.65
Pressure drop (Atm)	4.5
Water temperature increase (°C)	30

2.1 Tests and Mechanical measurements

A set of electrical and hydraulic measurements [5] has been performed on the prototype. The measured values are very close to the design ones. The major discrepancy is the nominal current (702 A instead of 675 A). The gap between the poles, without magnetic field, varies between 40.12 mm and 40.17 mm.

The attractive force produced by the magnetic field reduces the gap by 0.35 mm (with a standard deviation of 0.05 mm), as predicted by 3-D simulation, and corresponds to about 34 tons. The vertical parts of the four "C" side ribbings, directly supported by four jacks, do not move (negligible compression): the yoke movements are due to the combination of bending and rotation of the "C" ribbings.

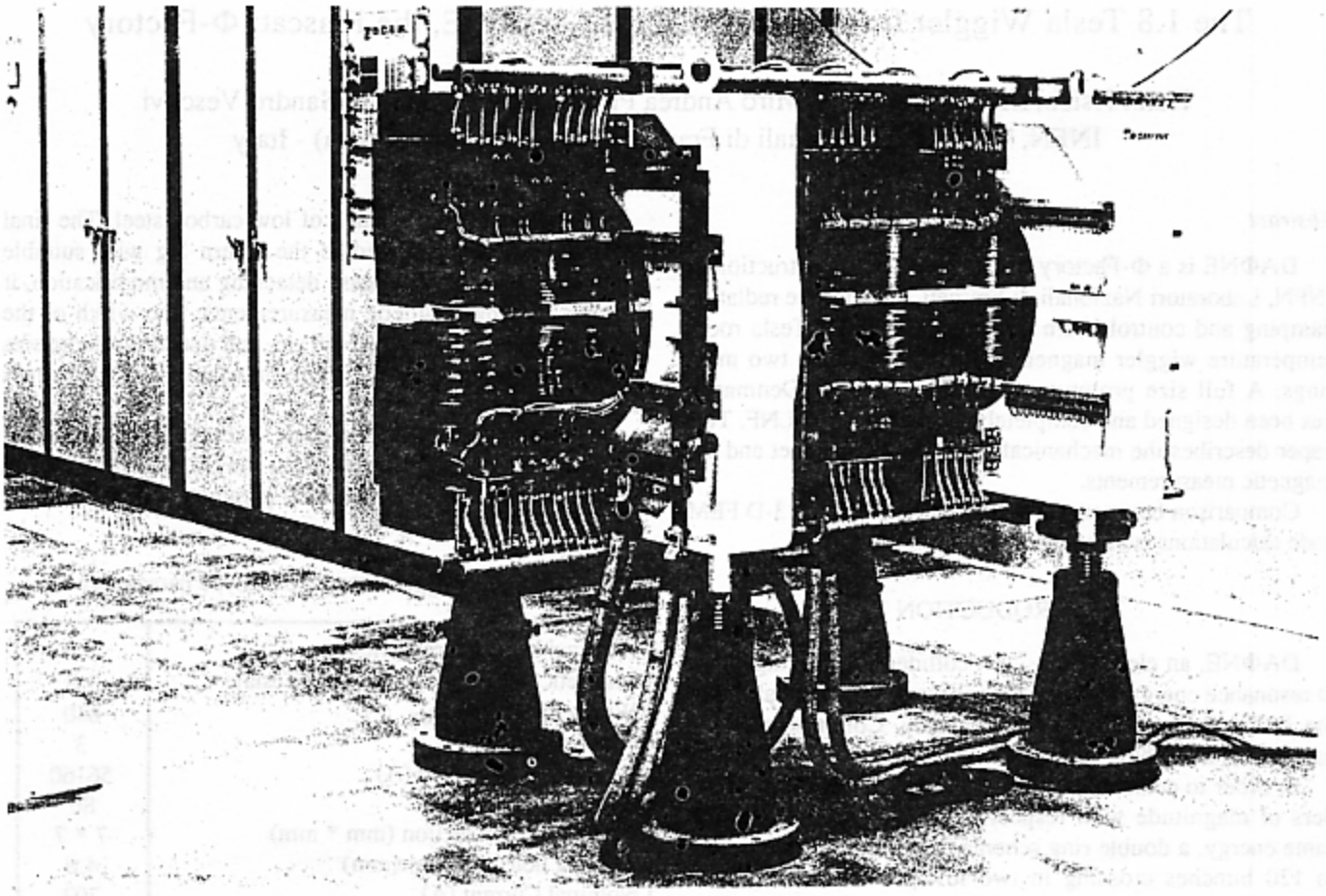

Figure 1. Wiggler prototype.

3. MAGNETIC MEASUREMENTS

A first set of measurements [5] with a 3 m long flip-coil has been performed, in order to rapidly find the current in the end poles required to make the field integral vanish on the wiggler axis as a function of the current in the main poles. Compensation on the particle trajectory is much more cumbersome, since one has to perform point to point measurements on the wiggler horizontal symmetry plane and integrate the equation of motion of the electrons in the measured field. An exact solution can be found only after a certain number of iterations. Due to the limited width of the poles (14 cm) and the large amplitude of the oscillating trajectory inside it (≈2.5 cm), the wiggler will be displaced towards the outside of the ring by half this amplitude. In this case the field integrals on the trajectory and on the wiggler axis have the same value within the required closed orbit tolerance.

Figure 2 shows the current in the end poles and the maximum field in the main poles measured with a Hall probe as a function of the current in the main poles. probe can be displaced horizontally and vertically in 5 mm steps by means of precision pins on the carriage.

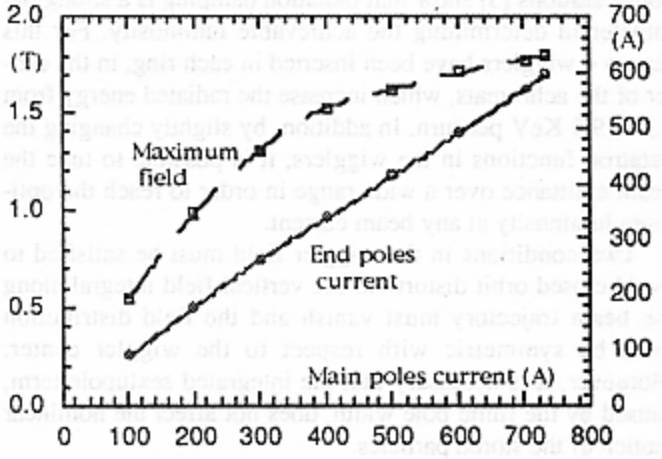

Figure 2. End poles compensation curve.

The behaviour of the field as a function of longitudinal, horizontal and vertical position inside the wiggler has been investigated by means of a Hall probe (Bruker B-H15 Teslameter) calibrated against a NMR (Metrolab PT2025) device. The probe is mounted on a pneumatically suspended carriage in a reference guiding box.

The longitudinal position of the probe is monitored by an encoder with 0.1 mm resolution, and the Figure 3 shows the vertical field distribution on the wiggler axis. The compensation curve of Figure 2 has been checked at the maximum field and at a few intermediate points by integrating the point-to-point measurements, and found in agreement within ≈10 A in the end pole current. Repeatability of the integrated field in a longitudinal scan has been found to be within ±1 Gm.The dependence of the integrated field on the horizontal coordinate gives an estimate of the sextupole term in the wiggler field expansion.

Figure 4 shows the result of the measurement, where the second order best fit yields a sextupole integrated term of -2.2 T/m, about ten times smaller than the contribution of a chromaticity correcting sextupole.

Numerical simulations have shown that the perturbation introduced by the wiggler is not harmful to the nonlinear behaviour of the particles in the rings. The symmetry of the field with respect to the wiggler center has been found to be within 50 G at the maximum excitation. Again, numerical simulations have shown that the effect on the closed orbit is negligible.

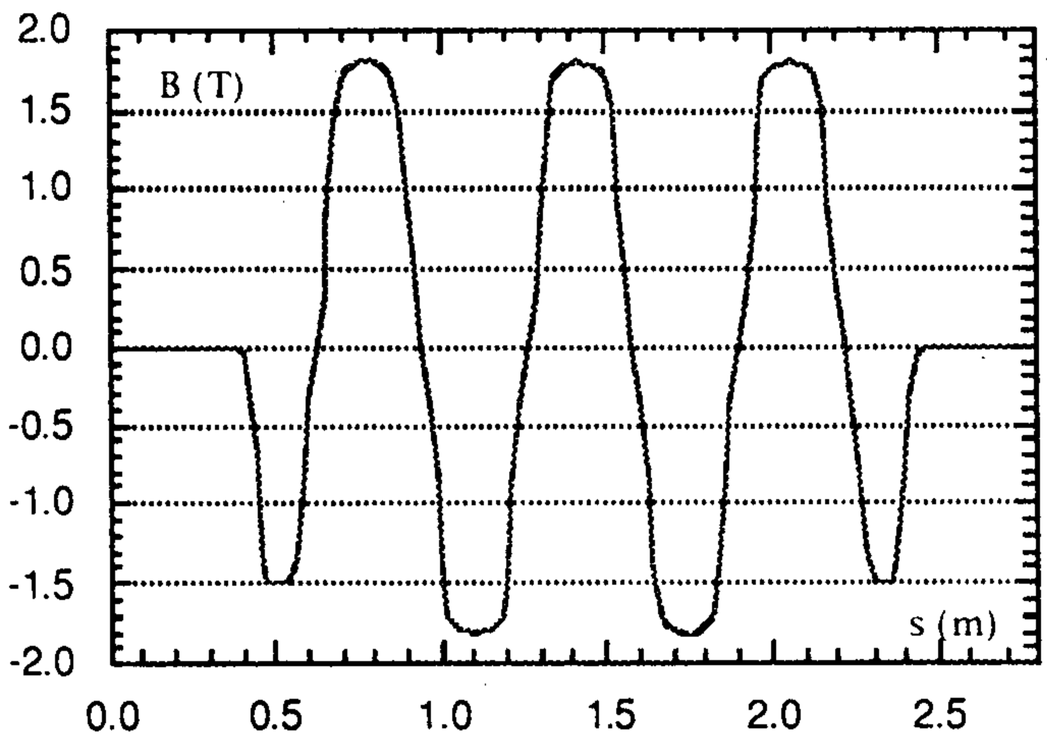

Figure 3. Vertical field along the wiggler axis

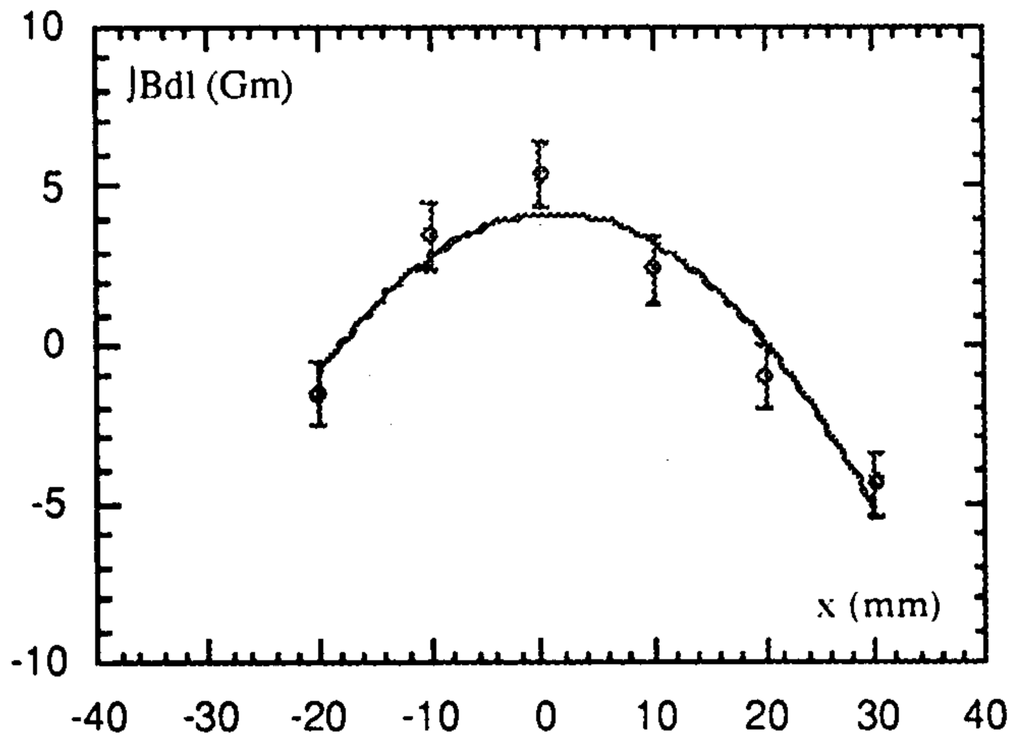

Figure 4. Integrated sextupole term in the wiggler field.

4. Comparison with Magnetic F.E.M. Design

We have compared the measured field with the prediction of the 3-D finite element code MAGNUS [6] in a section of the wiggler starting from the midpoint of the last full pole, going through the end pole and the field clamp, and ending up in the fringing field region.

Figure 5 shows the calculated field (line) and superimposed experimental points (dots): the agreement is quite satisfactory.

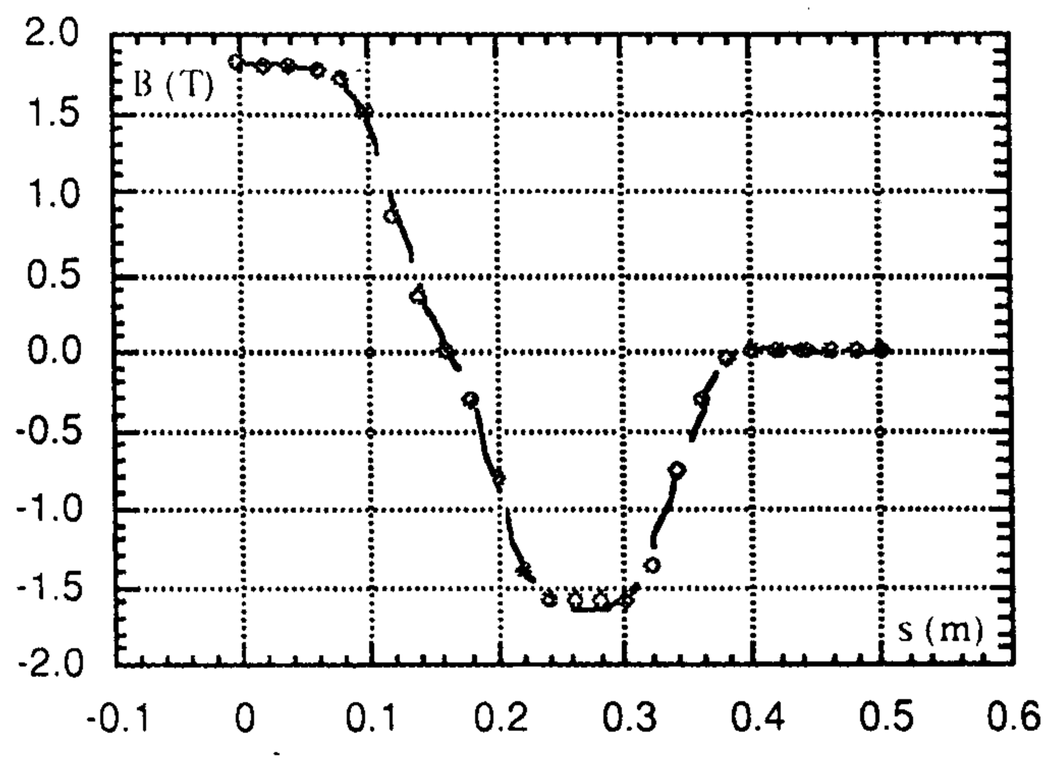

Figure 5. Comparison between measured and calculated field

5. Conclusions

A complete set of mechanical, electrical, hydraulic and magnetic tests has been performed of the prototype wiggler magnet delivered by Danfysik to LNF in January 1994. These tests have suggested a number of modifications to be developed on the final version of the magnet and the power supplies. Using both a rotating coil system and a Hall probe driven by an accurate positioning system, the field integral on the wiggler axis has been carefully compensated at several operating points. Although some asymmetries in the field and a non-negligible sextupole term have been evidenced by the measurements, we feel confident that the magnetic quality of the wiggler meets the requirements of the DAΦNE Main Rings.

3. References

[1] The DAΦNE Project Team, "DAΦNE, the Frascati Φ-Factory", 1993 Particle Accelerator Conference, Washington, USA, May 1993, p. 1993.

[2] J. Seeman, "Observations of the Beam-Beam Interaction", Nonlinear Dynamics Aspects of Particle Accelerators, Sardinia, Italy, February 1985, p.121.

[3] M. Bassetti, LNF Technical Note ARES-18, October 1989.

[4] C. Sanelli and H. Hsieh, "Design of the 1.8 Tesla Wiggler for the DAΦNE Main Rings" EPAC 92, 3rd European Particle Accelerator Conference, Berlin-Germany, March 1992, Proc. Vol. II p. 1391.

[5] B. Bolli, F. Iungo, M. Modena, M.A. Preger, C. Sanelli, F. Sgamma, S. Vescovi, "Measurements on the wiggler magnet for the DAΦNE Main Rings", DAΦNE Technical Note M-4, April 1994.

[6] The MAGNUS Package - Ferrari Associates, Inc. - P.O. Box 1866, Orange Park FL 32067 USA.

Single Electron Operation Mode in DAΦNE BTF

A. Ghigo and F. Sannibale
INFN, Laboratori Nazionali di Frascati - 00044 Frascati (Roma) - Italy

Abstract

The DAΦNE Beam Test Facility (BTF) [1] will use the LINAC-beam parasitically injection into the collider. It is a beam transfer line which has been designed in order to optimize the operation mode in which single electrons are stochastically produced for detector calibration purposes. The system consists of a metallic target intercepting the LINAC beam followed by an 'Energy Selector System' (ESS). The target strongly increases the beam energy spread, while the ESS selects the beam reducing the number of electrons in the bunches. Fine tuning is achieved by trimming focusing elements in the line. The facility is now under construction and the final design is presented.

1. INTRODUCTION

The injector of the DAΦNE accelerator complex [2] is a LINAC delivering electron and positron beams with a maximum energy of 800 MeV and 550 MeV respectively. Between two consecutive injections these beams can be switched on a special transfer line, the BTF, for the production of single particle pulses. Such beams are useful for the calibration of particle detectors used in high energy physics experiments. It is worth remarking that pulses of single electrons have already been obtained at Orsay with a system similar to the one described here [3] and also at CERN with a different approach [4].

2. BASIC PRINCIPLES

2.1. Beam-target Interaction

A relativistic electron (or positron) passing through matter loses energy mainly through two processes: ionization and radiation loss. The ratio between these two different losses is a function of the electron energy and of the material and can be roughly expressed by [5]:

$$\frac{\left(\frac{\partial E}{\partial x}\right)_{RAD}}{\left(\frac{\partial E}{\partial x}\right)_{ION}} \approx \frac{Z E_o}{800} \tag{1}$$

where E is the electron energy in MeV, x the material thickness, Z the atomic number of the material and E_O the initial electron energy in MeV. For copper (Z=29), and a 500 MeV electron the ratio is ≈18, indicating that the radiation loss dominates. In this situation it is reasonable to neglect the ionization term, assuming that the electron loses energy only through radiation.

The energy distribution w of an electron (positron) of initial energy E_O after passing through a target of α radiation lengths thickness, is given, with good approximation, by [6]:

$$w(E_o, \alpha, E) = \frac{1}{E_o} \frac{\left[ln\left(\frac{E_o}{E}\right)\right]^{\frac{\alpha}{ln\,2}-1}}{\Gamma\left(\frac{\alpha}{ln\,2}\right)} \tag{2}$$

where $\Gamma(x)$ is the gamma function. The probability P to find the electron with energy in the interval $[E_O - \Delta E, E_O]$, with $\Delta E \ll E_O$, is given by:

$$P = \frac{1}{2\,\Gamma\left(\frac{\alpha}{ln\,2}\right)} \left[ln\left(\frac{1}{1-\frac{\Delta E}{E_o}}\right)\right]^{\frac{\alpha}{ln\,2}-1} \frac{\Delta E}{E_o} \tag{3}$$

where the factor 1/2 comes from the arithmetic average between the values of (2) in $E_O - \Delta E$ and E_O. Furthermore, since again $\Delta E \ll E_O$, it is possible to write, with good approximation, that:

$$P = \frac{1}{2\,\Gamma\left(\frac{\alpha}{ln\,2}\right)} \left(\frac{\Delta E}{E_o}\right)^{\frac{\alpha}{ln\,2}} \tag{4}$$

As a conclusion, for a bunch of N electrons or positrons with energy E_O passing through a target of α radiation lengths, the average number of outgoing particles with energy in the range $[E_O - \Delta E, E_O]$ will be:

$$N_{\Delta E} = N\,P \tag{5}$$

2.2. Energy Selection

The Energy Selector System (ESS) is the device which selects, from the whole bunch, only the particles satisfying condition (5).

As shown in Figure 1, the system consists of a 45° DC sector bending magnet (DHSTB01) with a vertical slit in its focus (SLTTB01) and with a second slit upstream the magnet (SLTTM01). The energy acceptance of the ESS can then be easily derived:

$$\left|\frac{\Delta E}{E}\right| = \frac{h_F}{2\rho} + \sqrt{2}\,\left|x_o'\right|_{MAX} \tag{6}$$

where ρ is the bending magnet radius, h_F the total aperture of the slit in the magnet focus and $\left|x_o'\right|_{MAX}$ the maximum horizontal divergence the particle can have at the magnet entrance.

The latter can be limited by the slit upstream the magnet:

$$|x_o'|_{MAX} = \frac{\sigma_x^T + h_U/2}{l} \qquad (7)$$

where h_U is the total slit aperture, l is the target-slit distance and σ_x^T the beam radius at the target output. This cut on maximum divergence is necessary because the beam-target interaction dramatically increases the beam emittance.

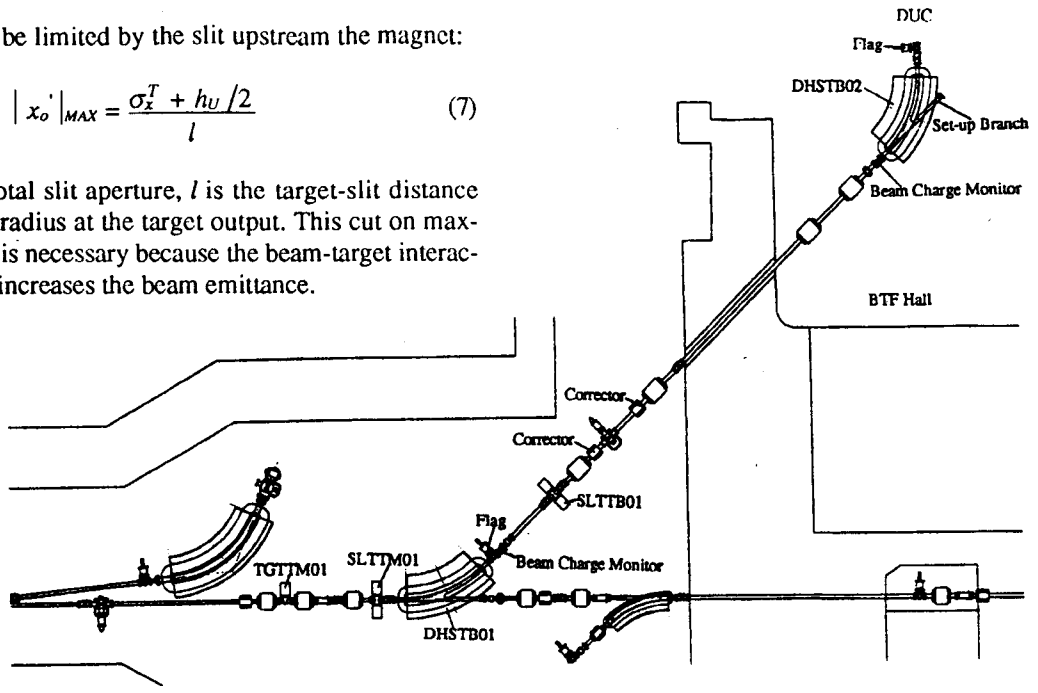

Figure 1. BTF General Lay-Out.

To give an idea of the magnitude of the selection factors involved in the production of a single electron pulse, we describe here the case of the BTF at 500 MeV.

First we set the LINAC to deliver a 500 MeV electron beam with the minimum current diagnostic system is able to detect (≈1 mA averaged over the 10 ns FWHM macrobunch), corresponding to:

$$N = 6.2 \times 10^7 \text{ particles} \qquad (8)$$

ρ and l are 1.722 m 1.499 m respectively, and the expected beam radius at the target input face is 1.2 mm. The passage through the $\alpha = 2$ radiation lengths target enlarges the beam by a factor ≈3 (a more detailed estimate can be given by the EGS code [7]) and thus $\sigma_x^T \approx 4$ mm. Setting $h_U = 8$ mm, $h_F =$ 8.5 mm and using expressions (6) and (7), we obtain an ESS energy acceptance:

$$\left|\frac{\Delta E}{E}\right| = 1\ \% \qquad (9)$$

and from (4):

$$P = 4.7 \times 10^{-7} \qquad (10)$$

Finally, using (5) and (8), we get:

$$N_{\Delta E} \approx 30 \qquad (11)$$

2.3. Fine Tuning

Expression (11) indicates that, in order to achieve $N_{\Delta E} = 1$ for the average number of electrons with energy E = (500 ± 3) MeV, fine tuning is necessary. In practice an adjustment of this kind is always necessary and can be performed following several methods.

The simplest are:
- Trimming of the LINAC gun current.
- Proper setting of the LINAC focusing system.

2.4. Statistical Considerations and Error Analysis

The number of particles within the selected energy range follows the Poisson distribution:

$$P_m(k) = e^{-m}\,\frac{m^k}{k!} \qquad (12)$$

where $m = N_{\Delta E}$. This means that when the BTF is properly set (m=1), it delivers ≈37% of the pulses with a single electron, ≈37 % with no electrons, ≈18% with two electrons and ≈8% with more than two electrons.

From another point of view ≈59% of the non empty pulses carry a single electron. It is worth remarking that, setting $m < 1$, the number of empty pulses increases but the ratio of single electron pulses over the non empty ones increases as well. For example, if $m = 0.5$, then ≈80% of the non empty pulses carry a single electron.

In order to estimate the sensitivity of m to the variation of the system parameters it is necessary to differentiate expression (5), taking (4) into account. After some algebra, it can be found that:

$$\frac{\Delta m}{m} = \frac{\Delta N}{N} + \frac{\alpha}{\ln 2}\left[\frac{\Delta E_o}{E_o} + \frac{\Delta(\Delta E)}{(\Delta E)} + \left|\ln\left(\frac{\Delta E}{E_o}\right) - \psi\left(\frac{\alpha}{\ln 2}\right)\right|\frac{\Delta\alpha}{\alpha}\right] \qquad (13)$$

where $\psi(x)$ is the digamma function. Let us now consider the meaning of each error contribution.

$\Delta N/N$: fluctuation of the number of particles per pulse. This is determined mainly by the gun stability.

$\Delta E_o / E_o$: LINAC beam central energy fluctuation: RF and trigger systems stability.

$\Delta\alpha / \alpha$: target thickness error. The dependence of (13) on this term is quite strong. The target surfaces must be carefully machined to minimize this error. It is worth pointing out that, for a given surface finishing, the use of a larger radiation length material decreases this error contribution.

$\Delta(\Delta E)/(\Delta E)$ describes the fluctuations of the range selected by the ESS. It can be expressed, using (6), as:

$$\frac{\Delta(\Delta E)}{(\Delta E)} = \frac{\Delta E_o}{E_o} + \frac{1}{1 + \frac{2\sqrt{2}\,\rho\,|\dot{x_0}|_{MAX}}{h_F}} \left(\frac{\Delta h_F}{h_F} + \frac{\Delta \rho}{\rho} \right) + \frac{1}{1 + \frac{h_F}{2\sqrt{2}\,\rho\,|\dot{x_0}|_{MAX}}} \frac{\Delta |\dot{x_0}|_{MAX}}{|\dot{x_0}|_{MAX}} \qquad (14)$$

with:

$$\frac{\Delta |\dot{x_0}|_{MAX}}{|\dot{x_0}|_{MAX}} = \frac{\Delta l}{l} + \frac{1}{1 + \frac{2\sigma_x^T}{h_U}} \frac{\Delta h_U}{h_U} + \frac{1}{1 + \frac{h_U}{2\sigma_x^T}} \frac{\Delta \sigma_x^T}{\sigma_x^T} \qquad (15)$$

where:

$\Delta h_F / h_F$: variations of h_F due to slit inner faces parallelism and finishing errors.

$\Delta\rho / \rho$: bending radius variations mainly due to the power supply current fluctuations.

$\Delta l / l$: this error appears when the output face of the target is not parallel to the input face of the slit upstream the dipole magnet.

$\Delta\sigma_x^T / \sigma_x^T$: the beam spot variation comes mainly from the fluctuations of the focusing magnets power supply current.

$\Delta h_U / h_U$: variations of h_U due to slit inner faces parallelism and finishing errors.

The dependence of the Poisson distribution (12) on m is:

$$\frac{\Delta P_m(k)}{P_m(k)} = e^{-\Delta m} \left(1 + \frac{\Delta m}{m} \right)^k - 1 \qquad (16)$$

and, in particular, if $k = 1$, $m \approx 1$ and $\Delta m / m < 15\ \%$ then:

$$\frac{\Delta P_m(1)}{P_m(1)} \approx \frac{1}{2} \left(\frac{\Delta m}{m} \right)^2 \qquad (17)$$

These expressions allow to estimate the effects of the tolerances (mechanical, electrical, etc.) on the system stability. The BTF has been designed to yield $\Delta m / m < 10\%$ and therefore the overall system stability (17) is better than 1%.

3. THE BTF TRANSFER LINE AND DIAGNOSTICS

The BTF lay-out is shown in Figure 1. The LINAC beam comes from the left side and strikes the removable copper target (TGTTMO1). Three different thicknesses can be selected: 1.7, 2.0 and 2.3 radiation lengths.

A change of one order of magnitude per thickness step in the value of P given by expression (4) is therefore possible. Downstream the target, the beam goes into the ESS (see §2.2) and after energy selection the remaining particles are driven into a room outside the LINAC vault where the detector under calibration (DUC) can be placed. This choice allows to isolate the DUC from the strong noise coming from the LINAC vault.

The dipole magnet DHSTB02, identical to DHSTB01, can send the beam on the DUC (magnet ON) or in a special small branch (magnet OFF) where a single particle detector, probably a lead glass, is used to set the BTF without damaging the DUC.

The BTF transfer line focusing system consists of four quadrupoles and a complete diagnostic set including 2 beam charge monitors, 2 fluorescent flags and 2 horizontal and vertical correctors, which will be useful in setting the line before the insertion of the target.

4. REFERENCES

[1] F. Sannibale, G. Vignola, "DAΦNE-LINAC Test Beam", DAΦNE Technical Note LC-2, October 29, 1991.

[2] The DAΦNE Project Team, "DAΦNE, the Frascati Φ–factory" in 1993 Particle Accelerator Conference, Washington D.C., USA, May 1993, pp. 1993-1997.

[3] Orsay Linear Accelerator Group, Private Communications.

[4] L. Rinolfi, "Single Electron Project" CERN PS/LP Note 88-66, August 16, 1988.

[5] E. Fermi, "Nuclear Physics" The University of Chicago Press (1949).

[6] B. Rossi, "High Energy Particles" Prentice-Hall, Inc. Englewood Cliffs, N.J.

[7] W.R. Nelson, H.Hiramaya and D.W.O.Roger, "The EGS4 code system" SLAC-PUB 265,1985.

A 3rd Harmonic Cavity for DAΦNE

S. Bartalucci, M. Migliorati, L. Palumbo*, B. Spataro, M. Zobov
INFN Laboratori Nazionali di Frascati, C.P. 13 - 00044 Frascati (Rome) - Italy
*Dipartimento di Energetica , Università di Roma 'La Sapienza', Via A. Scarpa 14, 00161 Rome - Italy

Abstract

In order to control bunch length in the DAΦNE main rings [1] an active 3rd harmonic RF cavity has been proposed. The energy acceptance, bunch length and Landau damping of the multibunch instabilities with the cavity are discussed. Alternative cavity shapes optimized with the aim of reducing the number of dangerous HOMs and increasing the fundamental mode shunt resistance are presented.

1. INTRODUCTION

The longitudinal size of a single bunch in storage rings is of great importance for reaching high luminosity. In order to avoid geometrical luminosity reductions the bunch length has to be shorter than $\beta_y/1.5$ [2], where β_y is the vertical betatron function at the interaction point. On the other hand, a too short bunch produces strong parasitic losses, fast multibunch instabilities, and short Touschek lifetime. For DAΦNE, a bunch length of 3 cm has been chosen as a reasonable compromise.

Preliminary calculations on the bunch lengthening have shown that the final bunch length in DAΦNE is less than 3 cm; therefore additional lengthening is necessary [3]. A third harmonic cavity is planned to be installed in the DAΦNE storage rings for this purpose.

In this paper we investigate the influence of the third harmonic cavity on the beam dynamics. The bunch lengthening (shortening) in the double RF system is computed taking into account the longitudinal broad-band impedance calculated elsewhere [3]. A simple analytical formula to estimate the enhancement of Landau damping of multibunch instability due to the cavity is derived. The last section is devoted to the discussion of possible cavity shapes with particular attention to the minimization of both the dissipated RF power and the number of dangerous HOMs.

2. BUNCH LENGTH

The potential seen by a particle in a double RF system, consisting of a main RF cavity and a n^{th} harmonic cavity, is given by [4, 5, 6]:

$$\varphi(\tau) = \frac{\alpha_c}{(E/e)T_o}\frac{\hat{V}_g}{\omega}\left[\sin(\varphi_{so}) \pm \frac{k}{n} - \sin(\varphi_{so} - \omega\tau) \mp \right. \qquad (1)$$
$$\left. \mp \frac{k}{n}\cos(n\omega\tau) - (U_o/e)\tau\right]$$

with α_c the momentum compaction, E the nominal energy of the particle, T_o the revolution period, $\hat{V}_g$ peak voltage in the main RF cavity, $k\hat{V}_g$ the peak voltage in the harmonic cavity, U_o the energy loss per turn. In order to provide phase stability the synchronous phase φ_{so} must satisfy the condition:

$$\mp\frac{kn}{\sin\varphi_{so}} < 1 \qquad (2)$$

The potential (1) is written for the case when the harmonic cavity does not accelerate synchronous particles and has a maximum voltage slope at $\varphi = \varphi_{s0}$ to have the most effective bunch length control. The upper sign in (1) and in the following refers to the shortening regime, while the lower one is used for the bunch lengthening case.

Applying the general theory of RF acceleration [7], we find that the relative change of the momentum acceptance due to the third harmonic cavity in a storage ring ($\varphi_{so} \sim \pi/2$):

$$\frac{\Delta E_{double}}{\Delta E_{main}} = \sqrt{1 \pm \frac{k}{3}} \qquad (3)$$

does not exceed ±6% if k < 1/3. Here ΔE_{double} and ΔE_{main} are the heights of the bucket in the double RF system and in the single one, respectively.

The "natural" bunch length in the double RF system is computed by solving Haissinski's equation [8] for the potential (1) with zero broad-band impedance. In the linear approximation and expressing the voltage of the harmonic cavity in terms of the supplied power P and the shunt impedance of the fundamental mode R_S the rms bunch length is:

$$\sigma = \sigma_o \Big/ \sqrt{1 \pm \frac{n\sqrt{2R_sP}}{\hat{V}_g\sin(\varphi_{so})}} \qquad (4)$$

In Fig. 1 we plot the normalized bunch length versus k in the case of a third harmonic cavity at different values of σ_o. As obtained in the linear approximation, for short bunches the ratio σ/σ_o does not depend on σ_o, while for longer bunches σ/σ_o is rather sensitive to σ_o. Nevertheless, in the range of interest defined by (2) the approximation is quite accurate.

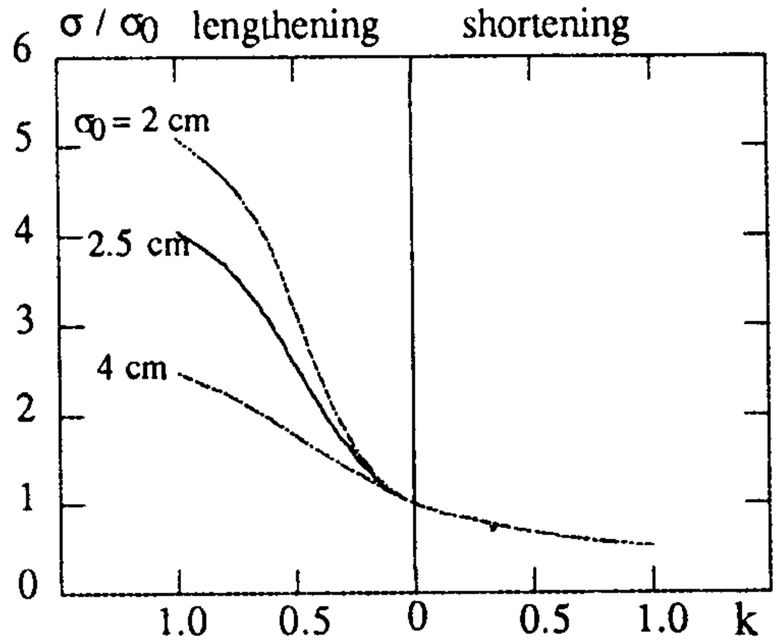

Figure 1. Bunch length versus k.

The bunch length (4) has been used as starting point to evaluate the bunch lengthening with the longitudinal impedance estimated for DAΦNE. Above the turbulent threshold the bunch length was calculated by solving Haissinski's equation and applying Boussard's criterion [9] as a scaling law as described in [10]. Figure 3 shows the bunch length versus power for different values of the shunt impedance.

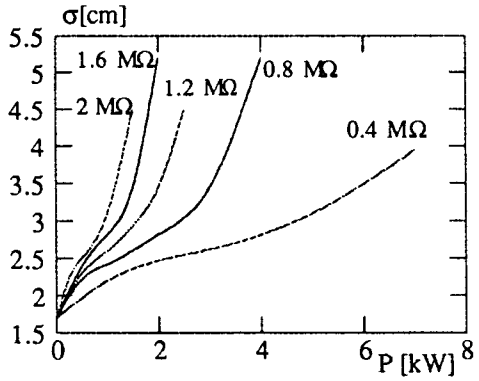

Figure 2. Bunch length versus dissipated power.

3. LANDAU DAMPING

The higher harmonic cavity introduces some additional non-linearities on the restoring force, which increase the synchrotron frequency spread, thus stabilizing the multibunch coherent oscillations through the Landau damping mechanism.

In order to estimate this effect, we use the Vlasov's equation linearized with respect to small perturbations of the stationary distribution [11,12] and get the dispersion integral:

$$1 = \frac{jm\alpha_c I_b}{(E/e)\omega_s(0)} \frac{Z(p)}{p} \int_o^\infty \frac{\partial g(\hat{\tau})}{\partial \hat{\tau}} \frac{J_m^2[p\omega_o\hat{\tau}]}{[\omega_{cm} - m\omega_s(\hat{\tau})]} d\hat{\tau} \quad (5)$$

where m is the mode number of oscillation, I_b the average beam current, $\omega_s(\hat{\tau})$ the incoherent synchrotron frequency, $\hat{\tau}$ the amplitude of the synchrotron oscillation, $Z(p)$ the longitudinal HOM shunt impedance at the frequency $p\omega_o + m\omega_{cm}$, p an integer number, ω_o the revolution angular frequency, ω_{cm} the coherent synchrotron frequency, $g(\hat{\tau})$ the stationary distribution in phase space, and J_m the Bessel function of the first kind of the mth order.

The dependence $\omega_s(\hat{\tau})$ is found by solving the equation of motion of a single particle in the potential (1). Using a perturbation method [13] and limiting ourselves to the first approximation which is suitable for the DAΦNE parameters we obtain:

$$\omega_s(\hat{\tau}) = \omega_{so}\sqrt{1 \pm \frac{kn}{\sin\varphi_{so}}}\left\{1 - \frac{0.0625(\omega\hat{\tau})^2}{\left(1 \pm \frac{kn}{\sin\varphi_{so}}\right)}\left(1 \pm \frac{kn^3}{\sin\varphi_{so}}\right)\right\}$$

By substituting $\omega_s(\hat{\tau})$ in the dispersion integral we get for the Gaussian stationary distribution:

$$\frac{Z(p)}{p} = F\frac{E\pi\omega_{so}^2\sigma^2\omega^2}{4el_b\alpha_c}\left\{\frac{\pm\pi e^{-y}J_m^2[p\omega_o\sigma\sqrt{2y}] + j\Im_{pv}}{\Im_{pv}^2 + \left(\pi e^{-y}J_m^2[p\omega_o\sigma\sqrt{2y}]\right)^2}\right\} \quad (6)$$

where $\Im_{pv}$ is the principal value of the integral:

$$\Im_{pv} = PV\int_o^\infty \frac{e^{-x}J_m^2[p\omega_o\sigma\sqrt{2x}]}{x-y}dx \text{ , and } F = 1 \pm \frac{kn^3}{\sin\varphi_{so}}$$

and y a function depending on ω_{cm}. The sign + or - in the double bracket depends on whether F is positive or negative respectively. Examining eq.(6) we find that, in presence of a higher harmonic cavity, there is an enhancement of the Landau damping by a factor F, whose maximum value in the lengthening regime is $n^2 - 1$.

4. CAVITY DESIGN

We describe two basic alternative designs for the higher harmonic cavity, which were explored to fulfill different requirements, i. e.:

1) 'Single-mode' cavity, to have minimum contribution to the HOM impedance in DAΦNE.

2) High shunt impedance cavity, either of the 'nosecone' or of the 'rounded' type, to keep RF power to a minimum.

We remind that the beam pipe aperture is quite large (a radius of 4.3 cm), and does not allow us to push the R_S of the fundamental mode to a very big value at the third harmonic frequency. In this work we used the well-known codes URMEL [14] and TBCI [15].

4.1. Nosecone cavity

A 'nosecone' design was considered as a possible solution to have a true single mode cavity (see Fig. 3).

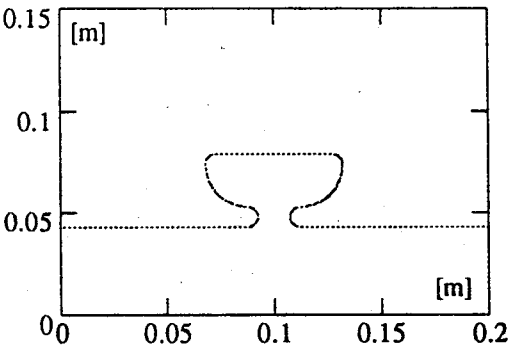

Figure 3. Nosecone 'single-mode' cavity.

We studied the cell shape for several gap values, keeping the frequency of the fundamental mode at 1104 MHz. The cell is set directly on the pipe and the elliptical profile helps to shift the two first HOMs above cutoff, while the nose radius was chosen large enough not to have a too high surface electric field. In this way something is lost on the R_S/Q but all the monopole modes look free to propagate down the vacuum chamber. It can be generally said that only the first dipole mode TM_{110} is left in such a cavity. The other dipole mode TE_{111} practically disappears (see Table 1).

Construction and cooling of such a cavity may be difficult, due to its rather complicated geometry and reduced size. Tolerances for a construction error of ± 0.1 mm have been calculated by simulation for the most critical positions [16].

The cavity does not appear too sensitive from this point of view. The maximum tuner sensitivity calculated assuming a cylindrical tuner of 1.5 cm radius is given in Table 1.

Table 1 - Summary results for the cavities

	Nosecone (gap=15mm)	Nosecone High Rs	Rounded High Rs
Frequency (MHz)	1104.57	1104.59	1104.71
R_S/Q (Ω)	33.38	58.73	65.36
R_S (MΩ)	0.335	1.96	1.85
V_{gap} (kV)	75	75	75
W (mJoule)	12.13	6.2	6.9
E_S max (MV/m)	9.5	2.8	1.97
B_S max (Gauss)	114	29	30.6
Tuner sensitivity (mm/MHz)	0.6	4.7	4.8
k [V/pC]	0.0699	0.171	0.157
k_{pm} [V/pC]	0.000	0.0453	0.017
TM_{011} mode:			
Frequency (MHz)	propagating	1839.61	1916.26
R_S (kΩ)	------	612.0	672.6
TM_{020} mode:			
Frequency (MHz)	propagating	2429.	2342.
R_S (kΩ)	------	4.7	7.6
TM_{110} mode:			
Frequency (MHz)	1601.	1644.	1604.
R'_S(kΩ)(at 4.3cm)	266.	366.	299.
TE_{111} mode:			
Frequency (MHz)	2020.	1453.7	1412.6
R'_S(kΩ)(at 4.3cm)	0.416	84.6	150.3

4.2. Rounded and Nosecone High R_S cells

To minimize RF power, high R_S structures were considered too. First, a rounded profile (Fig. 4) was chosen with the optimum value $a/h \sim 1$ [17], obtaining R_S = 1.85 MΩ and 4 (monopole + dipole) trapped modes, which have to be damped anyway.

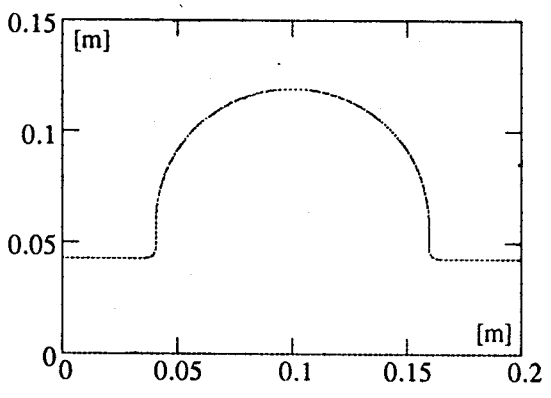

Figure 4. Rounded high R_S cell.

Second, a quite optimized nosecone cell (Fig. 5) was accurately studied by re-adjusting the gap, to get maximum R_S/Q and simultaneously not to decrease Q. The resulting R_S is 1.96 MΩ at 1104 MHz. Also in this case 4 parasitic modes are left in the cavity. The cavities are less sensitive to construction errors than the nosecone cavity described in 4.1.

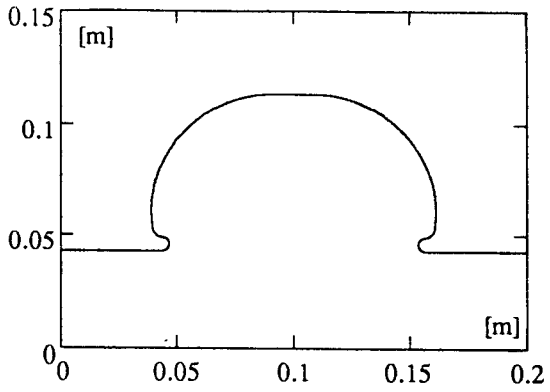

Figure 5. Nosecone high R_S cell.

All the described cavities comply (within at least a factor 10) with Kilpatrick's criterion on the maximum surface electric field [18]. A summary of the most important results is reported in Table 1.

5. CONCLUSIONS

Bunch lengthening in DAΦNE with the double RF system has been studied. We have shown that a shunt impedance of R_S = 0.3+2 MΩ allows to keep the bunch length in DAΦNE under control with reasonable RF power (1+7 kW) while variations of the momentum acceptance do not exceed ±6%. All the cavities shown have the necessary shunt impedance. The final choice will be made after careful analysis of the means to damp undesired HOMs. We also found that a high harmonic cavity gives an enhancement of the Landau damping effect by a factor $\left(1 \pm kn^3 / \sin \varphi_{so}\right)$, beneficial for damping the multibunch instability.

6. REFERENCES

[1] The DAΦNE Project Team, "DAΦNE: The Frascati Φ-Factory", in Particle Accelerator Conference, Washington DC, USA, May 1993, p. 1993.
[2] M.A. Preger, in European Particle Accelerator Conference, Berlin, Germany, March 1992, p. 385.
[3] M. Migliorati, et al., DAΦNE Technical Note G-22, Frascati, November 1993.
[4] P. Bramham, et al., LEP/70-25, December 1977.
[5] A. Hofmann, S. Myers, LEP Note 158, June 1979.
[6] Y. Ho Chin, LBL-29622, November 1990.
[7] G. Dôme, CERN Accelerator School 87-03, p.110.
[8] J. Haissinski, Il Nuovo Cimento, Vol. 18B, N.1
[9] D. Boussard CERN-Lab II/RF/75-2 (1975).
[10] K. Bane, SLAC-PUB-5177, February 1990 (A).
[11] J. L. Laclare, CERN 87-03, Vol. I, p. 264.
[12] M. Migliorati, et al., DAΦNE Technical Note G-21, Frascati, September 1993.
[13] N.N. Bogoliubov, Y.A. Mitropolsky, "Asymptotic Methods in the Theory of Non-Linear Oscillations", Hindustan Publishing Corpn. (India), 1961.
[14] T. Weiland, NIM 216 (1983), p. 329.
[15] T. Weiland, NIM 212 (1983), p. 13.
[16] S. Bartalucci, B.Spataro, DAΦNE Technical Note RF-12, Frascati, May 1994.
[17] S.Bartalucci, B.Spataro, DAΦNE Technical Note RF-10, Frascati, October 1993.
[18] W. P. Kilpatrick, VCRL - 2321, Sept. 1953.

Solenoidal Compensation Scheme for an Interaction Region of an Electron-Positron Collider

M. Bassetti, C. Biscari, C. Milardi
INFN, Laboratori Nazionali di Frascati - 00044 Frascati (Roma) - Italy

Abstract

Solenoidal fields of detectors in colliders are compensated usually with the 4 skew quadrupole method, which is not optimal for Φ-factories. In DAΦNE the Rotating Frame Method [1] has been adopted. An alternative compensation scheme, with a small superconducting solenoid, providing also final focusing at the interaction point, is described. The optical aspects of a possible application to one of the DAΦNE Interaction Regions are discussed.

1. INTRODUCTION

In high energy rings experimental detectors need often solenoidal fields which must be compensated to avoid coupling between horizontal and vertical oscillations [1,2,3].

When the beam energy is relatively low, like in Φ-factories, the coupling introduced by the experimental solenoid may be so strong that it becomes one of the main optical characteristics of the ring.

In DAΦNE [1,4] rotation of each low beta quadrupole and compensating superconducting solenoids provide cancellation of coupling outside the interaction regions (IRs).

In the Novosibirsk Φ-factory project [5] the solenoidal coupling is not compensated but used specifically to generate emittance in the two transverse phase spaces and to focus the round beam.

We present here a new idea for a compensating method which we have applied as an example to the DAΦNE IR which houses the detector of the FI.NU:DA. [6] experiment.

2. THE NEW COMPENSATION SCHEME

The basic idea of this scheme starts from the observation that the total optical effect of a rectangular field model solenoid can be split in two completely different effects (see Appendix). The first one is a rotation of the transverse plane by the angle:

$$\theta_r = \frac{B_z L_s}{2B\rho} \qquad (1)$$

where L_s is the solenoid length, B_z its longitudinal field, and $B\rho$ the magnetic rigidity of the beam. The second one is a focusing quadrupole effect on both planes characterized by the quadrupole constant K_s:

$$K_s = \frac{B_z}{2B\rho} \qquad (2)$$

The focusing properties of a quadrupole for each plane are determined by the element A_{21} of the 2x2 transport matrix. For a solenoid (see Appendix):

$$A_{21} = -K_s \sin\theta r \approx -\frac{\theta_r^2}{L_s} \qquad (3)$$

The last formula is the key point. For the same longitudinal field integral, proportional to θ_r, the focusing effect is inversely proportional to the solenoid length.

The new scheme can be imagined as derived from the DAΦNE scheme [1] by interchanging the positions of the quadrupoles and the compensator. The compensator placed inside the detector very near to the Interaction Point (IP) can have a small radius. Furthermore its length can be very small to increase its focusing properties on both planes.

An advantage of this scheme is that the coupling vanishes at all energies within the beam energy spread.

On each side of the IP two quadrupoles instead of four are enough to properly focus the beam at the crossing point and match the optical functions to the arcs outside the detector. Of course they do not need any rotation and can be realized as conventional electromagnets.

The solution studied for FI.NU.DA. is based on the preliminary experiment design parameters, recalled in the following table.

Table I - FI.NU.DA. detector characteristics

Total integrated field ($B_z L_s$, Tm)	3
Maximum field (B_{max}, T)	1.1
Total length (L_s, m)	2.7
Total rotation angle (θ_r, deg)	50.05

The FI.NU.DA. detector needs a region free from machine components defined by two 45° half aperture cones with the vertex at ~20cm from the IP, outside which the compensator solenoid can be housed.

Computations have been performed on a 22 cm superconducting coil . The inner radius is 6 cm and the outer 7 cm, corresponding to ≈550 A/mm^2 current density. The required beam stay clear aperture inside the compensator is a circle of 3.5 cm radius, based on the assumption of $10\sigma_x$ (off coupling) and $10\sigma_y$ (full coupling) as a limit for good quantum lifetime [7], crossing angle ±15 mrad, vertical separation @ IP of ±2.5 mm. Therefore there are 2.5 cm left for the vacuum chamber and helium circulation.

The optical functions behaviour in half IR is shown in Figure 1 together with the beam trajectory for a crossing angle of ±10 mrad. The longitudinal magnetic field inside the detector is plotted in Figure 2, together with the rotation angle of the betatron oscillation planes.

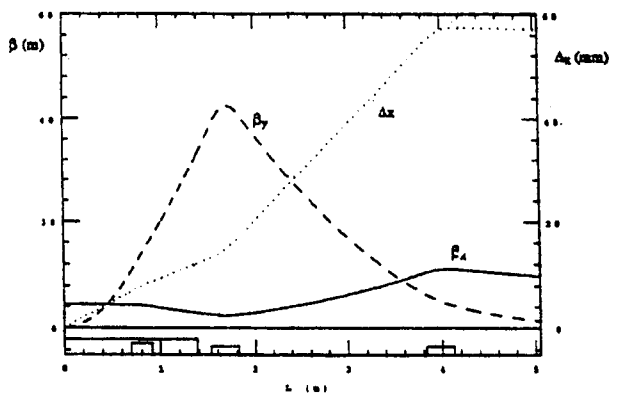

Figure 1. Optical functions and beam central trajectory in half IR

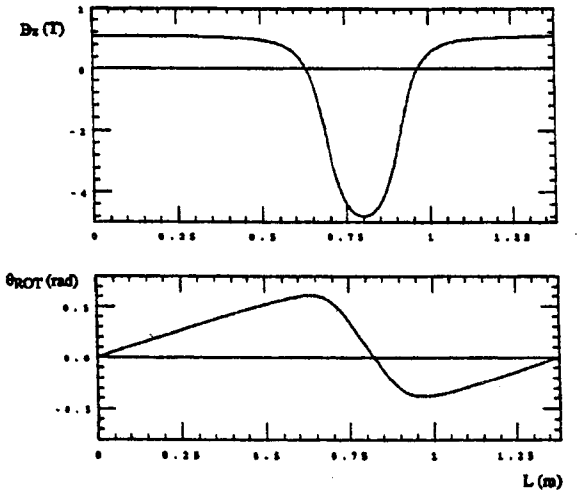

Figure 2. Total longitudinal magnetic field in the detector region and total rotation angle

If the detector field is changed to follow experimental requirements, the compensating solenoid field has to be changed accordingly to maintain the compensation (this is not possible in the previous scheme with quadrupoles unless each one can be rotated independently inside the detector). From the optics point of view the focusing effect is an increasing function of the ratio between the detector field and the beam rigidity. The quadrupoles are therefore used to compensate the variation of the detector-compensator focusing in order to keep the IP β functions and matching the ring arcs constant. The natural chromaticity of the whole ring is, however, lower at high solenoid and compensator fields and the dynamic aperture is larger as well. On the contrary the IR optics is almost unperturbed if the detector is switched off. The two compensating solenoids must be oppositely powered, at a field $|B|=|B_c|-|B_d|$ where B_c and B_d are the nominal operating fields of the compensator and the detector respectively.

3. MAGNETIC FIELD ANALYSIS

The analysis of the magnetic properties of the detector plus compensator system has been carried out, under the assumption of a constant field in the main detector solenoid with the compensator coil superimposed without any iron contribution.

Due to the cylindrical symmetry of the model the magnetic field is two-dimensional and therefore its effect on the lattice can be estimated more accurately than in the standard rectangular approximation.

The longitudinal and radial magnetic field profiles of the compensator are shown in Figure 3 along half main detector solenoid. The plots show the field on axis and on concentric surfaces of different radius. It can be observed that the longitudinal field decreases rapidly with the distance from the axis: B_z is of the order of 10% of the value on axis at r = 10 cm. The magnetic lines of force for half IR are shown in Figure 4: it is clear that the detector field is not affected inside the 45° cone.

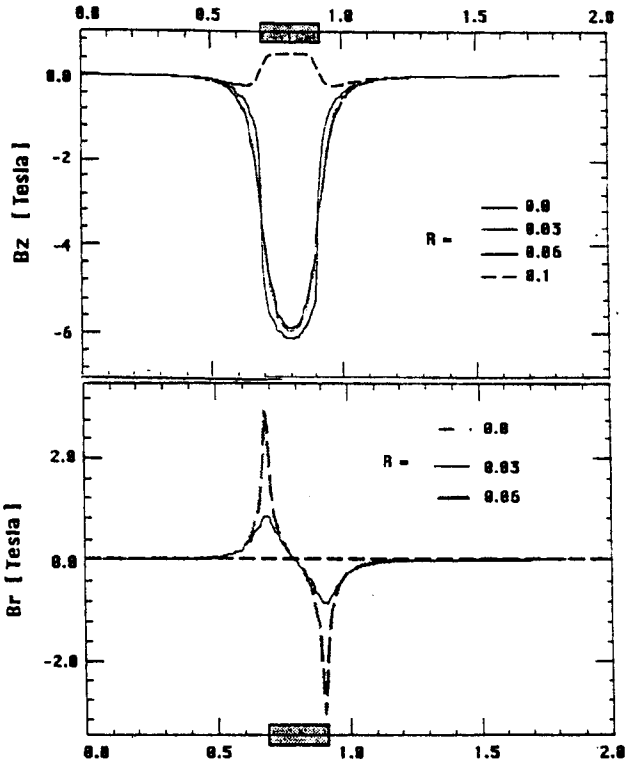

Figure 3. Longitudinal and radial magnetic field of the compensating solenoid along the detector length

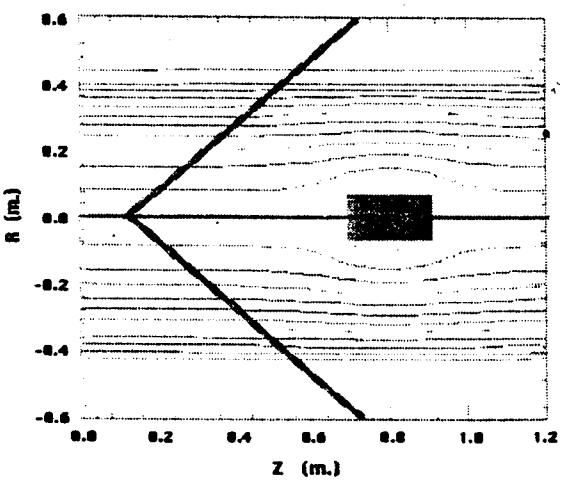

Figure 4. Magnetic lines of force with main detector and compensator solenoids

4. ANALYTICAL COMPUTATIONS

A tracking code has been developed where the particle trajectories are computed as solutions of the three-dimensional equations corresponding to the motion of relativistic particles inside the total magnetic field.

In order to solve the equations, the Jacobian around the particle trajectory has been computed and used as the transport matrix corresponding to the whole detector zone. This matrix, whose simplecticity has been checked, can be used in kick codes. A similar result can be found by multiplicating many matrices, each representing a very small solenoid chunk. We found a good agreement between the two different approaches.

The analysis of the Jacobian around the axis verifies (as expected) that the horizontal and vertical oscillations are uncoupled. The Jacobian around the actual particle trajectory, which makes an angle of 12.5 mrad with respect the magnet axis at the IP, shows a small coupling never exceeding the project value of 1%.

APPENDIX - OPTICAL PROPERTIES OF SOLENOIDS

Defining:

$$K_S = \frac{B_z}{2B_r} \tag{4}$$

and

$$\theta_r = K_S L_S \tag{5}$$

the transport matrix corresponding to the rectangular model solenoid can be written for both transverse planes as:

$$Q_S = \begin{vmatrix} \cos\theta_r A & \sin\theta_r A \\ \sin\theta_r A & \cos\theta_r A \end{vmatrix}$$

where **A** is the 2x2 matrix:

$$A = \begin{vmatrix} \cos\theta_r & \frac{\sin\theta_r}{K_S} \\ -K_S \sin\theta_r & \cos\theta_r \end{vmatrix}$$

Defining matrices **R** and **F** as:

$$R(\theta_r) = \begin{vmatrix} \cos\theta_r \, I & \sin\theta_r \, I \\ -\sin\theta_r \, I & \cos\theta_r \, I \end{vmatrix}$$

$$F(L_S,\theta_r) = \begin{vmatrix} A & 0 \\ 0 & A \end{vmatrix}$$

we can also write:

$$Q_S = R\,F = F\,R \tag{6}$$

The conclusion is that a solenoid has focusing and rotating effect in both planes. Its contribution to the chromaticity is larger by a factor 2 with respect to a quadrupole with the same length and the same focusing strength, because of the different energy dependence.

Expressing the integrated solenoid focusing strength as a function of the rotation angle:

$$K_S^2 L_S = -\frac{\theta_r^2}{L_S} \tag{7}$$

we notice that while θ_r depends only on the integrated B_Z, the focusing strength, at a given θ_r, is inversely proportional to L_S. This explains why the focusing properties of the small compensating solenoid are so relevant while those of the main detector with the same absolute value of θ_r are negligible.

This rectangular model is exact only in the limit of a uniform field shape, which is true when the ratio between the internal radius and the total length is small, or when the magnetic field is clamped by the iron joke (like in the DAΦNE detectors).

In a more general case the optical effects of a longitudinal magnetic field can be computed or by tracking or by decomposing it in thin slices, each represented in the rectangular model.

REFERENCES

[1] M. Bassetti et al,"DAΦNE Interaction Region Design" in 1193 Particle Accelerator Conference, Washington, USA, May 1993, p. 2048.

[2] G. Guignard, "Revised schemes of skew-quadrupoles for solenoid compensation in LEP", LEP-70/75.

[3] M. Bassetti, J.P. Koutchouk, "The compensation of the solenoidal perturbation (an alternative computation), LEP Note 631, 6 Nov. 1990.

[4] C. Biscari, "FI.NU.DA IR Preliminary Design"- Technical DAΦNE Note L-15, May 1994.

[5] L. Barkov et al., Novosibirsk "Project of Φ-Meson Factory" Proceedings of Workshop on Physics and Detectors for DAΦNE - Frascati, April 9-12 1991, p. 67.

[6] The FI.NU.DA. Collaboration, LNF-93/021(IR), May 1993.

[7] C. Biscari, "DAΦNE Stay-Clear Aperture", Technical Note DAΦNE L-6.